Buckling-resistant thin annular plates in tension

Ciprian D Coman and Xiang Liu

Mathematics and Mechanics of Solids 2014 19: 925 originally published online 8 August 2013
DOI: 10.1177/1081286513493108

Article

MMS

Mathematics and Mechanics of Solids
2014, Vol. 19(8) 925–951

DOI: 10.1177/1081286513493108
mms.sagepub.com

SAGE

Buckling-resistant thin annular plates in tension

Ciprian D Coman
Schlumberger Gould Research, High Cross, Cambridge, UK

Xiang Liu
University of Glasgow, School of Mathematics and Statistics, Glasgow, UK

Received 4 May 2013; accepted 16 May 2013

Abstract

Motivated by the localized nature of elastic instabilities in radially stretched thin annular plates, we investigate the resistance to buckling of such configurations in the case when their mechanical properties are piecewise constant. By considering a plate consisting of two sub-annular regions perfectly bonded together and with different linear elastic properties, the neutral stability envelope corresponding to the case when radial constant displacement fields are applied on the inner and outer edges of the plate is investigated numerically in considerable detail. These results are complemented by an asymptotic reduction strategy that provides a greatly simplified eigenproblem capable of describing the original buckling problem in the limit of very thin plates.

Keywords

Thin plates, wrinkling, variational methods, WKB methods

1. Introduction

The design of slender structures capable of withstanding significant loads without the risk of instability or mechanical failure represents one of the central problems in structural mechanics. Elastic or plastic buckling is a common type of instability to which many thin structural elements, such as plates or shells, are prone. Some possible solutions for improving the structural strength of these configurations involve the use of stiffening ribs or strings and fibre-reinforced materials.

Numerical and experimental results by Geminard et al. [1] have indicated that thin annular elastic plates uniformly stretched by constant displacement fields applied on their edges are susceptible to a localized form of buckling near the central hole. This deformation has a regular character in the azimuthal direction, with the rest of the originally flat configuration experiencing little or no deformation at all. A comprehensive analytical investigation of this problem was undertaken by the first author and his associates (see [2, 3]); all of these studies were carried out within the framework of plates with homogeneous elastic properties. Given the localized nature of the elastic instability, the question arises as to whether a plate with piecewise-constant mechanical properties, as in Figure 1, would lead to a more efficient design. This is the question that motivated the present study.

Corresponding author:
Ciprian D Coman, Schlumberger Gould Research, High Cross, Madingley Road, Cambridge CB3 0EL, UK.
Email: cdc3p@yahoo.com

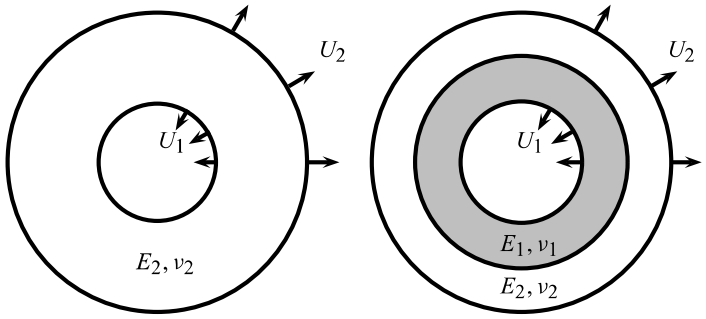

Figure 1. Two different annular configurations under the same uniform stretching displacement fields U_1 and U_2. The left sketch shows a homogeneous annular plate with material constants E_2, ν_2, while on the right the plate has piecewise-constant mechanical properties.

Configurations such as those seen in the right-hand sketch of Figure 1 are sometimes known in the literature as *bi-annular plates*. The terminology comes from the fact that the plate itself consists of two concentric sub-annular plates bonded along a common interface. Buckling of bi-annular plates subjected to global compressive in-plane forces was studied in some detail by Frostig and Simitses [4, 5] (see also [6]), with the help of direct numerical simulations and power-series methods. A perfect bond was assumed to exist between the two sub-regions in their first papers, while in [5] the authors dealt with detailed parametric studies for the buckling of ring-stiffened annular plates under compression, and discussed the effect of boundary conditions and various plate/ring rigidity constants on this phenomenon. However, the emphasis in their work was mostly on instability modes that were either axisymmetric ($n = 0$) or asymmetric ($n = 1$) because the buckling instability had a more or less diffuse character. Some vibration problems for bi-annular elastic plates were also explored by Stavsky and Greenberg [7, 8].

As shown in the already-mentioned studies of the first author, the localized buckling of the stretched annular plate was due to a standard plane-stress concentration phenomenon associated with the presence of the geometric discontinuity (the central hole). In a stretched bi-annular plate this stress concentration is likely to be more complicated due to its piecewise-constant mechanical properties. As a consequence, the localized buckling might be confined to the outer sub-annular region rather than near the central hole.

It must be pointed out that the matters discussed in this paper are essentially different from the apparently related buckling problems involving multi-span beams or plates studied extensively by Elishakoff et al. [9] (see also the references therein). In that work localized classical buckling (i.e. under compressive loads) was discovered to be present in plates periodically reinforced by stiffeners when some small miss-alignment was present. Not only is the physical nature of those instabilities unrelated to the stress concentration that underlies our problem, but also the mathematical techniques employed by those authors are significantly simpler as they only had to deal with constant-coefficient differential equations.

To address the various questions that surface in relation to extending the work of Coman and Haughton [2] for the case of a bi-annular configuration, we take the following route. After a brief introduction of the problem in Section 2, we proceed to a quick review of the variational formulation of Trefftz' criterion in Section 2.1 in order to establish the matching conditions for the solutions of the linearized Föppl–von Kármán equations in the two subparts of the plate; the earlier studies by Frostig and Simitses [4, 5] seem to contain some errors regarding this aspect. The resulting eigenproblem is then reduced to a three-point boundary-value problem for a fourth-order ordinary differential equation by using the standard normal-mode approach. Suitable rescaling introduces a non-dimensional parameter $\mu > 0$ (such that its reciprocal plays the role of bending rigidity) and suggests that the limit $\mu \gg 1$ is of interest for very thin plates. Since possible buckling instabilities originate in the presence of compressive azimuthal stresses, we undertake a detailed analysis of the possible stress concentration phenomena for the basic state (corresponding to $\mu = \infty$). As shown by Coman [10], this already reveals a fairly rich behaviour that includes the possibility of having disjoint plate regions working in compression. A similar situation was encountered in the plane-strain analyses for bending of a rubber cuboid described by Roccabianca et al. [11, 12]. In that section we also provide an analytical criterion that helps identify certain features that bear on the qualitative properties of the response curves (Section 4.1) and the neutral stability envelope (Section 4.2) discussed in the next sections. It is these latter aspects that make the present problem

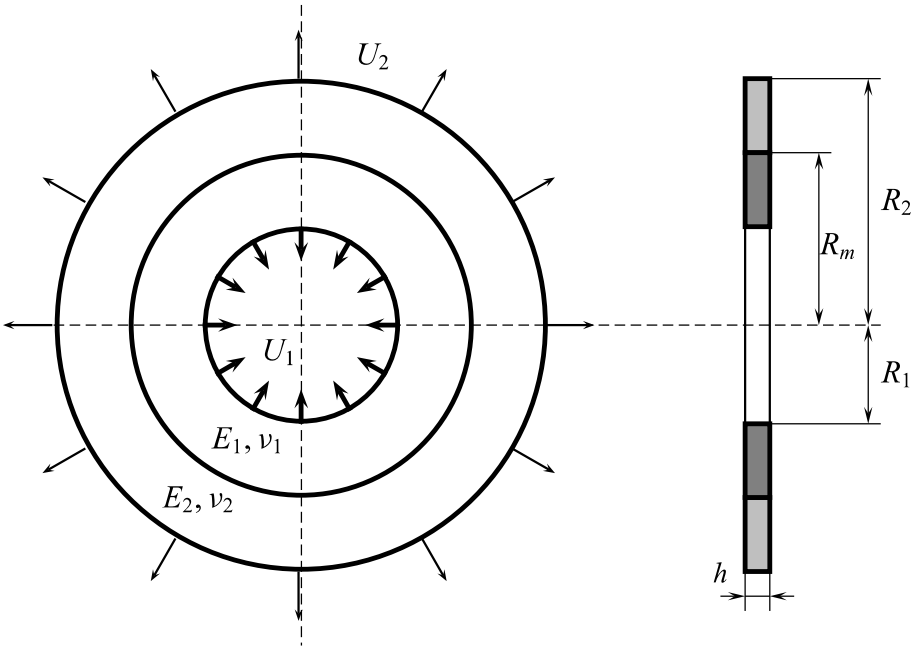

Figure 2. A bi-annular plate stretched by applying uniform displacement fields on both its inner and outer edges. The two constituent parts Ω_I and Ω_{II} are assumed to be perfectly bonded together.

rather different from the earlier results obtained by Coman and Haughton [2]. Unlike in that study, here we discover that the neutral stability curves need not be convex, a fact that corresponds to the possibility of localization in either sub-annular region. A detailed numerical study is carried out in Section 4, where we pay special attention to the question addressed at the beginning of this introductory section. Finally, Section 5 provides the rudiments of an asymptotic strategy that permits the reduction to a second-order model of the complicated fourth-order equations for the bi-annular plate. Comparisons with direct numerical simulations of the original problem show excellent agreement when $\mu \gg 1$, thus confirming the robustness of the reduced models. Such reduced models open the possibility for a WKB analysis involving differential equations with discontinuous coefficients. With the exception of the excellent work by Steele and Skogh [13], who employed such methods in the context of shells of revolution with meridional slope discontinuity, the topic appears to be rather unexplored in the solid mechanics literature. The first author has showed in a recent study [10] that WKB methods can be used effectively in conjunction with the simplified equations mentioned above in order to provide analytical approximations for the critical loads.

2. Problem formulation

Let us start by considering a simple plane-stress situation that generalizes the Lamé problem for an annular domain subjected to uniform radial stresses or displacements on its inner and outer boundaries. We shall consider a linearly elastic plate of uniform thickness $h > 0$ whose midplane is described by the two-dimensional annular region $\Omega \subset \mathbb{R}^2$. Rather than having homogeneous elastic properties, the annulus is assumed to consists of two perfectly bonded concentric annular regions, $\Omega_I := \{(r,\theta) \mid R_1 \le r \le R_m,\ 0 \le \theta < 2\pi\}$ and $\Omega_{II} := \{(r,\theta) \mid R_m \le r \le R_2,\ 0 \le \theta < 2\pi\}$ that have different mechanical properties. More precisely, we shall assume that $\Omega = \Omega_I \cup \Omega_{II}$ (details of the geometry that we have in mind can be seen in Figure 2). The material properties of Ω_I are characterized by Young's modulus E_1 and Poisson's ratio ν_1, while for Ω_{II} those constants are identified as E_2 and ν_2. The loading of this configuration is achieved by imposing the constant displacement fields U_1 (inward) and U_2 (outward) along the inner and outer rims, respectively.

2.1. Energy considerations in invariant form

The starting point of our analysis is the classical plate theory based on the Föppl–von Kármán kinematics. Given the presence of the interface inside Ω, the usual boundary conditions on the outer edges of the plate will have to be supplemented by an appropriate set of constraints along $r = R_m$. It will turn out that in addition to the usual kinematic conditions (the continuity of the out-of-plane displacements and the slopes of the deformed plate mid-surface along that interface), one needs to consider a set of extra equations akin to the Weierstrass–Erdmann conditions for "broken extremals" in the calculus of variations (e.g. see Gelfand and Fomin [14]). It must be pointed out that, although the out-of-plane displacements and their derivatives are continuous along $r = R_m$, we do allow for discontinuities in the curvature of the plate mid-surface.

We could take advantage of the polar symmetry of our annular configuration and carry out all calculations in component form, but here we prefer to employ a more elegant invariant approach that could be easily adapted for other similar problems in different geometries. The only assumption we make explicitly is that one of the coordinate axes is perpendicular to the plate midplane, and the corresponding coordinate will be identified as $-h/2 \le z \le h/2$. In agreement with the Love–Kirchhoff hypothesis for thin plates, the three-dimensional displacement field of material points in $\Omega \times \left[-\frac{h}{2}, \frac{h}{2}\right]$, denoted by $\boldsymbol{u}$, is expressed as $\boldsymbol{u} = \boldsymbol{v} - z\nabla w + w\widehat{\boldsymbol{n}}$, where $\boldsymbol{v}$ and w denote the in-plane and out-of-plane displacements, respectively, experienced by the plate midplane (both fields are defined on $\Omega \subset \mathbb{R}^2$). Here $\widehat{\boldsymbol{n}}$ is the unit normal to the plate midplane and ∇ represents the projection of the usual (three-dimensional) gradient operator onto this planar surface. As a result of this hypothesis the (reduced) Lagrange strain tensor is approximated by

$$\boldsymbol{E} \simeq (\nabla \otimes \boldsymbol{v})^s - z\nabla \otimes \nabla w + \frac{1}{2}(\nabla w) \otimes (\nabla w), \tag{1}$$

where $(\nabla \otimes \boldsymbol{v})^s \equiv (\nabla \otimes \boldsymbol{v} + \boldsymbol{v} \otimes \nabla)/2$.

The total strain energy consists of bending ($\mathcal{E}_b$) and stretching ($\mathcal{E}_s$) contributions, i.e. $\mathcal{E} = \mathcal{E}_b + \mathcal{E}_s$. If the material of the plate is assumed to be isotropic and linearly elastic, then the bending energy can be expressed in the form

$$\mathcal{E}_b(\boldsymbol{u}) := \frac{1}{2}D \int_\Omega \left\{(\nabla^2 w)^2 - (1-\nu)[w, w]\right\} \mathrm{d}A, \tag{2}$$

where D and ν are the bending stiffness and the Poisson's ratio, respectively (note that in our particular setting these will take on different values in Ω_I and Ω_{II}); the last term in the integrand stands for the Monge–Ampère bracket defined by $[f, g] := (\nabla^2 f)(\nabla^2 g) - (\nabla \otimes \nabla f) : (\nabla \otimes \nabla g)$.

It is also known that the stretching energy of plate midplane has the expression

$$\mathcal{E}_s(\boldsymbol{u}) := \int_\Omega \left[(\nabla \otimes \boldsymbol{v})^s + \frac{1}{2}(\nabla w) \otimes (\nabla w)\right] : \mathbb{C} : \left[(\nabla \otimes \boldsymbol{v})^s + \frac{1}{2}(\nabla w) \otimes (\nabla w)\right] \mathrm{d}A, \tag{3}$$

where $\mathbb{C}$ is the fourth-order stretching stiffness tensor whose components are

$$C^{\alpha\beta\gamma\delta} = \frac{Eh}{2(1+\nu)}\left[\frac{2\nu}{1-\nu} g^{\alpha\beta} g^{\gamma\delta} + g^{\alpha\gamma} g^{\beta\delta} + g^{\alpha\delta} g^{\beta\gamma}\right], \quad (\alpha, \beta, \gamma, \delta = 1, 2),$$

with $g^{\alpha\beta}$ the contravariant components of the two-dimensional (in-plane) identity tensor $\boldsymbol{I}$, and E denotes the usual Young's modulus.

The flat basic state is characterized by $\delta\mathcal{E} = 0$ for all variations of the displacement field which have no out-of-plane component and are compatible with the edge restraints. For the sake of clarity we shall use "$\mathring{}$" to denote the variables associated with the basic state. If an arbitrary variation is given to the flat configuration, that is $\mathring{\boldsymbol{u}} = \mathring{\boldsymbol{v}} + 0\widehat{\boldsymbol{n}} \to \mathring{\boldsymbol{v}} + t\boldsymbol{h}$, where $\boldsymbol{h} = \delta\mathring{\boldsymbol{v}} + 0\widehat{\boldsymbol{n}}$, then $\delta\mathcal{E}_b(\mathring{\boldsymbol{u}}) \equiv 0$ and

$$\delta\mathcal{E}_s(\mathring{\boldsymbol{u}})[\boldsymbol{h}] = 2\int_\Omega \mathring{\boldsymbol{N}} : \nabla \otimes (\delta\mathring{\boldsymbol{v}})\, \mathrm{d}A, \tag{4}$$

where $\mathring{\boldsymbol{N}} := \mathbb{C} : (\nabla \otimes \mathring{\boldsymbol{v}})^s$ represents the linearized membrane tensor in the pre-buckling state. On recalling the identity

$$\nabla \cdot (\boldsymbol{T} \cdot \boldsymbol{a}) = (\nabla \cdot \boldsymbol{T}) \cdot \boldsymbol{a} + \boldsymbol{T} : (\nabla \otimes \boldsymbol{a}), \tag{5}$$

valid for any second-order tensor and vector fields, $\boldsymbol{T}$ and $\boldsymbol{a}$, respectively, the equilibrium condition for the flat pre-stressed configuration can be recast using the divergence theorem,

$$\delta\mathcal{E}(\mathring{\boldsymbol{u}})[\boldsymbol{h}] \equiv \delta\mathcal{E}_s(\mathring{\boldsymbol{u}})[\boldsymbol{h}] = 2\int_{\partial\Omega}\left(\mathring{\boldsymbol{N}}\cdot\boldsymbol{n}\right)\cdot\delta\mathring{\boldsymbol{v}}\,\mathrm{d}S - 2\int_{\Omega}(\nabla\cdot\mathring{\boldsymbol{N}})\cdot\delta\mathring{\boldsymbol{v}}\,\mathrm{d}A = 0, \tag{6}$$

for any variations $\delta\mathring{\boldsymbol{v}}$ that satisfy the geometric boundary conditions. Hence, by using standard arguments, we finally conclude that $\nabla\cdot\mathring{\boldsymbol{N}} = \boldsymbol{0}$ in Ω.

To establish the variational structure of the buckling problem requires the consideration of three-dimensional variations around the stressed flat state. To this end, we shall assume displacement variations of the form $\mathring{\boldsymbol{u}} = \mathring{\boldsymbol{v}} + 0\widehat{\boldsymbol{n}} \to \boldsymbol{u} = \mathring{\boldsymbol{v}} + t\boldsymbol{h}$, where $\boldsymbol{h} = \delta\boldsymbol{v} + (\delta w)\widehat{\boldsymbol{n}}$. Routine calculations show that the second variation of the bending energy (2) is

$$\delta^2\mathcal{E}_b(\mathring{\boldsymbol{u}})[\boldsymbol{h}] = D\int_{\Omega}\left\{(\nabla^2(\delta w))^2 - (1-\nu)\,[\delta w, \delta w]\right\}\mathrm{d}A. \tag{7}$$

The counterpart of this formula for the stretching contribution is obtained by assuming that the membrane tensor $\mathring{\boldsymbol{N}}$ remains unchanged immediately before and after the buckling, so that

$$\delta^2\mathcal{E}_s(\mathring{\boldsymbol{u}})[\boldsymbol{h}] = \int_{\Omega}\mathring{\boldsymbol{N}} : \nabla(\delta w)\otimes\nabla(\delta w)\,\mathrm{d}A. \tag{8}$$

Adding the relations (7) and (8), we have

$$\delta^2\mathcal{E}(\mathring{\boldsymbol{u}})[\boldsymbol{h}] := D\int_{\Omega}\left\{(\nabla^2(\delta w))^2 - (1-\nu)[\delta w, \delta w]\right\}\mathrm{d}A + \int_{\Omega}\mathring{\boldsymbol{N}} : \nabla(\delta w)\otimes\nabla(\delta w)\,\mathrm{d}A. \tag{9}$$

According to the Trefftz criterion, in order to obtain the critical buckling state $\boldsymbol{u}_C$ we need $\delta\left(\delta^2\mathcal{E}(\mathring{\boldsymbol{u}})\right)[\boldsymbol{u}_C, \boldsymbol{h}] = 0$ for all $\boldsymbol{h} = \boldsymbol{v} + (w + t\delta w)\widehat{\boldsymbol{n}}$;[1] note that

$$\delta\left(\delta^2\mathcal{E}_b(\mathring{\boldsymbol{u}})\right)[\boldsymbol{u}_C, \boldsymbol{h}] \;\equiv\; 2D\int_{\Omega}\nabla^2 w\,\nabla^2(\delta w) \;-\; (1\;-\;\nu)\left[\nabla^2 w\,\nabla^2(\delta w) - (\nabla\otimes\nabla w) : (\nabla\otimes\nabla\delta w)\right]\mathrm{d}A. \tag{10}$$

Applying Green's first identity twice, $\int_{\Omega} f\nabla^2 g + \nabla f\cdot\nabla g\,\mathrm{d}A = \int_{\partial\Omega} f(\nabla g)\cdot\boldsymbol{n}\,\mathrm{d}S$, allows us to write

$$\int_{\Omega}\nabla^2 w\,\nabla^2(\delta w)\,\mathrm{d}A = \int_{\partial\Omega}\nabla^2 w\big[\nabla(\delta w)\cdot\boldsymbol{n}\big]\,\mathrm{d}S - \int_{\Omega}\nabla(\nabla^2 w)\cdot\nabla(\delta w)\,\mathrm{d}A \tag{11a}$$

$$= \int_{\partial\Omega}\nabla^2 w\,[\nabla(\delta w)\cdot\boldsymbol{n}]\;\mathrm{d}S - \int_{\partial\Omega}\big[\nabla(\nabla^2 w)\cdot\boldsymbol{n}\big]\delta w\,\mathrm{d}S + \int_{\Omega}(\nabla^4 w)\,\delta w\,\mathrm{d}A, \tag{11b}$$

where $\nabla^4 := \nabla^2(\nabla^2)$ stands for the usual bi-Laplacian. At the same time, we can transform further the last term that appears in (10),

$$\begin{aligned}
&\int_{\Omega}(\nabla\otimes\nabla w) : \big[\nabla\otimes\nabla(\delta w)\big]\,\mathrm{d}A\\
&= \int_{\Omega}\nabla\cdot\big[(\nabla\otimes\nabla w)\cdot\nabla(\delta w)\big]\,\mathrm{d}A - \int_{\Omega}\big[\nabla\cdot(\nabla\otimes\nabla w)\big]\cdot\nabla(\delta w)\,\mathrm{d}A\\
&= \int_{\partial\Omega}\Big[(\nabla\otimes\nabla w)\cdot\nabla(\delta w)\Big]\cdot\boldsymbol{n}\,\mathrm{d}A - \int_{\Omega}\nabla(\nabla^2 w)\cdot\nabla(\delta w)\,\mathrm{d}A,
\end{aligned} \tag{12}$$

where we have used again the identity (5) in writing the second line above, and the formula $\nabla\cdot(\nabla\otimes\nabla\phi) = \nabla(\nabla^2\phi)$ (valid for any scalar ϕ) was applied to obtain the last line.

If we take the first variation of (8), we have

$$\begin{aligned}\delta\left(\delta^2\mathcal{E}_s(\mathring{\boldsymbol{u}})\right)[\boldsymbol{u}_C,\boldsymbol{h}] &= 2\int_\Omega \mathring{\boldsymbol{N}} : [\nabla(\delta w)\otimes\nabla w]\,\mathrm{d}A = 2\int_\Omega \mathring{\boldsymbol{N}} : \nabla\otimes(\delta w\nabla w) - \mathring{\boldsymbol{N}} : (\nabla\otimes\nabla w)\delta w\,\mathrm{d}A\\ &= 2\int_\Omega \nabla\cdot(\mathring{\boldsymbol{N}}\cdot\delta w\nabla w) - \Big[(\nabla\cdot\mathring{\boldsymbol{N}})\cdot\nabla w\Big]\delta w - \mathring{\boldsymbol{N}} : (\nabla\otimes\nabla w)\,\delta w\,\mathrm{d}A\\ &= 2\int_{\partial\Omega}(\mathring{\boldsymbol{N}}\cdot\nabla w)\cdot\boldsymbol{n}\,\delta w\,\mathrm{d}S - 2\int_\Omega \mathring{\boldsymbol{N}} : (\nabla\otimes\nabla w)\,\delta w\,\mathrm{d}A,\end{aligned} \tag{13}$$

in which the identity $(\nabla\delta w)\otimes\nabla w = \nabla\otimes(\delta w\nabla w) - \delta w(\nabla\otimes\nabla w)$, Equation (5), and $\nabla\cdot\mathring{\boldsymbol{N}} = 0$ have been used in turn.

Putting together (10) and (13), by taking (11) and (12) into account, finally yields

$$\begin{aligned}\delta\left(\delta^2\mathcal{E}(\mathring{\boldsymbol{u}})\right)[\boldsymbol{u}_C,\boldsymbol{h}] &= 2\int_\Omega \left[D\nabla^4 w - \mathring{\boldsymbol{N}} : (\nabla\otimes\nabla w)\right]\delta w\,\mathrm{d}A\\ &\quad + 2D\int_{\partial\Omega}(1-\nu)\Big[(\nabla\otimes\nabla w)\cdot\nabla(\delta w)\Big]\cdot\boldsymbol{n} + \nu\nabla^2 w\,\nabla(\delta w)\cdot\boldsymbol{n}\,\mathrm{d}S\\ &\quad + 2\int_{\partial\Omega}\left[-D\nabla(\nabla^2 w) + \mathring{\boldsymbol{N}}\cdot\nabla w\right]\cdot\boldsymbol{n}\delta w\,\mathrm{d}S.\end{aligned} \tag{14}$$

If we consider a circular geometry, it is possible to cast the last equation in a more convenient form. The crucial observation is that in such a case the normal ($\boldsymbol{n}$) and tangential ($\boldsymbol{s}$) vectors to $\partial\Omega_{(j)}$ ($j\in\{I,II\}$) are scalar multiples of $\boldsymbol{e}_r$ and $\boldsymbol{e}_\theta$, respectively. By taking into account that $\nabla\otimes\boldsymbol{n} = 0$ and decomposing the second-order (in-plane) identity tensor as $\boldsymbol{I} := \boldsymbol{n}\otimes\boldsymbol{n} + \boldsymbol{s}\otimes\boldsymbol{s}$, we get

$$\begin{aligned}&\int_{\partial\Omega}(\nabla\otimes\nabla w)\cdot\nabla(\nabla w)\cdot\boldsymbol{n}\,\mathrm{d}S = \int_{\partial\Omega}(\nabla\otimes\nabla w)(\boldsymbol{n}\otimes\boldsymbol{n}+\boldsymbol{s}\otimes\boldsymbol{s})\cdot\nabla(\nabla w)\cdot\boldsymbol{n}\,\mathrm{d}S\\ &= \int_{\partial\Omega}(\nabla\otimes\nabla w)(\boldsymbol{n}\otimes\boldsymbol{n})\cdot\nabla(\nabla w)\cdot\boldsymbol{n} - \nabla\cdot\Big[(\boldsymbol{s}\otimes\boldsymbol{s})(\nabla\otimes\nabla w)\cdot\boldsymbol{n}\Big]\delta w\,\mathrm{d}S\\ &= \int_{\partial\Omega}(\nabla\otimes\nabla w)(\boldsymbol{n}\otimes\boldsymbol{n})\cdot\nabla(\nabla w)\cdot\boldsymbol{n} - \nabla\cdot\Big[(\boldsymbol{s}\otimes\boldsymbol{s})(\nabla\otimes\nabla w)\Big]\cdot\boldsymbol{n}\delta w\,\mathrm{d}S.\end{aligned}$$

Substituting the above into (14), the arbitrariness of δw and $\dfrac{\partial}{\partial n}(\delta w)$ will lead to

$$\int_\Omega\left[D\nabla^4 w - \mathring{\boldsymbol{N}} : (\nabla\otimes\nabla w)\right]\delta w\,\mathrm{d}A = 0, \tag{15a}$$

$$\int_{\partial\Omega}\left[-D\nabla(\nabla^2 w) - (1-\nu)\nabla\cdot\Big[(\boldsymbol{s}\otimes\boldsymbol{s})(\nabla\otimes\nabla w)\Big] + \mathring{\boldsymbol{N}}\cdot\nabla w\right]\cdot\boldsymbol{n}\delta w\,\mathrm{d}S = 0, \tag{15b}$$

$$\int_{\partial\Omega}(1-\nu)(\nabla\otimes\nabla w)(\boldsymbol{n}\otimes\boldsymbol{n})\cdot\nabla(\delta w)\cdot\boldsymbol{n} + \nu\nabla^2 w\nabla(\delta w)\cdot\boldsymbol{n}\,\mathrm{d}S = 0. \tag{15c}$$

Equations (15) must hold for all variations δw compatible with the boundary conditions for the out-of-plane displacements.

2.2. The boundary-value problem

At this stage we take further advantage of the circular symmetry of our problem to particularize the findings of the previous section. For obvious reasons we adopt a cylindrical system of coordinates with the origin at the

centre of Ω and the z-axis perpendicular to it. A number of useful operators that facilitate the notation later on are introduced below

$$\nabla_r := \frac{\partial}{\partial r}, \quad \nabla_\theta := \frac{1}{r}\frac{\partial}{\partial \theta}, \quad \nabla_{rr} := \frac{\partial^2}{\partial r^2}, \quad \nabla_{r\theta} := \frac{1}{r}\frac{\partial^2}{\partial r \partial \theta} - \frac{1}{r^2}\frac{\partial}{\partial \theta},$$
$$\nabla_{\theta\theta} := \frac{1}{r}\frac{\partial}{\partial r} + \frac{1}{r^2}\frac{\partial^2}{\partial \theta^2}, \quad \nabla^2 := \nabla_{rr} + \nabla_{\theta\theta}, \quad \boldsymbol{\nabla} := \begin{bmatrix} \nabla_r \\ \nabla_\theta \end{bmatrix}, \quad \boldsymbol{\nabla} \otimes \boldsymbol{\nabla} := \begin{bmatrix} \nabla_{rr} & \nabla_{r\theta} \\ \nabla_{r\theta} & \nabla_{\theta\theta} \end{bmatrix}. \tag{16}$$

The indices 'I' (or '1') and 'II' (or '2') will be employed in reference to quantities associated with Ω_I and Ω_{II}, respectively; in general, subscripts or superscripts meant to refer to these values will be placed between parentheses to avoid confusion with some of the tensor notation used in parallel. Also, C_j represents the boundary described by $r = R_j$ ($j = 1, 2$), while $C_m = \Omega_I \cap \Omega_{II}$.

As indicated by equation (6), the equilibrium of the basic state for the bi-annular plate requires

$$\delta\mathcal{E}(\mathring{\boldsymbol{u}})[\boldsymbol{h}] = 2\int_{C_1 \cup C_m} \left(\mathring{\boldsymbol{N}}^I \cdot \boldsymbol{n}^I\right) \cdot \delta\mathring{\boldsymbol{v}}^I \, \mathrm{d}S + 2\int_{C_2 \cup C_m} \left(\mathring{\boldsymbol{N}}^{II} \cdot \boldsymbol{n}^{II}\right) \cdot \delta\mathring{\boldsymbol{v}}^{II} \, \mathrm{d}S$$
$$- 2\int_{\Omega_I} (\boldsymbol{\nabla} \cdot \mathring{\boldsymbol{N}}^I) \cdot \delta\mathring{\boldsymbol{v}}^I \, \mathrm{d}A - 2\int_{\Omega_{II}} (\boldsymbol{\nabla} \cdot \mathring{\boldsymbol{N}}^{II}) \cdot \delta\mathring{\boldsymbol{v}}^{II} \, \mathrm{d}A = 0, \tag{17}$$

for all $\delta\mathring{\boldsymbol{v}}^{(j)}$ compatible with the geometric boundary conditions. We recall that $\mathring{\boldsymbol{v}}^I = -U_1\boldsymbol{e}_r$ along C_1, and $\mathring{\boldsymbol{v}}^{II} = U_2\boldsymbol{e}_r$ along C_2; hence, $\delta\mathring{\boldsymbol{v}}^{(j)} = 0$ on $C_1 \cup C_2$ and, as a result,

$$\boldsymbol{\nabla} \cdot \mathring{\boldsymbol{N}}^{(j)} \equiv \boldsymbol{0} \quad \text{in } \Omega_{(j)} \quad (j \in \{I, II\}). \tag{18}$$

These equations are readily solved by invoking the usual axisymmetry assumption $\mathring{N}_{r\theta} \equiv 0$ and $\mathring{N}_{rr} = \mathring{N}_{rr}(r)$, $\mathring{N}_{\theta\theta} = \mathring{N}_{\theta\theta}(r)$, together with $\mathring{\boldsymbol{v}} = \mathring{U}(r)\boldsymbol{e}_r$, for some function $\mathring{U}$ that is to be found. Note that the boundary conditions expressed in terms of this new function read

$$\mathring{U}^I(R_1) = -U_1 \quad \text{and} \quad \mathring{U}^{II}(R_2) = U_2. \tag{19}$$

The other matching conditions along the interface follow from (17) since $\mathring{\boldsymbol{v}}^I = \mathring{\boldsymbol{v}}^{II}$ and $\delta\mathring{\boldsymbol{v}}^I = \delta\mathring{\boldsymbol{v}}^{II}$ across C_m. By further taking into account that $\boldsymbol{n}^{II} = -\boldsymbol{n}^I = \boldsymbol{e}_r$ along C_m, Equation (17) becomes

$$\int_{C_m} \left[(\mathring{\boldsymbol{N}}^I - \mathring{\boldsymbol{N}}^{II}) \cdot \boldsymbol{n}^I\right] \cdot \delta\mathring{\boldsymbol{v}}^I \, \mathrm{d}S = 0, \quad \forall\, \delta\mathring{\boldsymbol{v}}^I$$

and this leads to the bracket in the integrand being zero. Since the thickness of both sub-annular regions is the same we can now summarize the constraints that are to be satisfied by the pre-buckling state in the form

$$\mathring{U}^I(R_m) = \mathring{U}^{II}(R_m) \quad \text{and} \quad \mathring{\sigma}^I_{rr}(R_m) = \mathring{\sigma}^{II}_{rr}(R_m). \tag{20}$$

Before solving the problem consisting of (18) and (20), it is found helpful to introduce a number of non-dimensional variables,

$$\rho := \frac{r}{R_2}, \quad \eta_1 := \frac{R_1}{R_2}, \quad \eta_2 := \frac{R_m}{R_2}, \quad \lambda := \frac{U_1}{U_2}, \quad \gamma := \frac{E_1}{E_2}, \tag{21a}$$

$$\mathring{\sigma}_{kk} \to \frac{1 - \nu_{(j)}^2}{E_{(j)}}\mathring{\sigma}_{kk}, \quad j \in \{1, 2\},\ k \in \{r, \theta\} \quad \text{(no sum over } k\text{)}, \tag{21b}$$

so that Ω is now defined by $\eta_1 \le \rho \le 1$ and the interface has equation $\rho = \eta_2$. Note that in Ω_I the independent variable $\rho \in \Lambda_I := [\eta_1, \eta_2]$, while in Ω_{II}, $\rho \in \Lambda_{II} := [\eta_2, 1]$.

The solution of the aforementioned pre-buckling problem can be represented in terms of the non-dimensional real constants $b^{(j)}$ and $c^{(j)}$ ($j \in \{I, II\}$) by the formulae

$$\begin{bmatrix} \mathring{\sigma}_{rr}^{(j)} \\ \mathring{\sigma}_{\theta\theta}^{(j)} \end{bmatrix} = \begin{bmatrix} 1+\nu_{(j)} & -\dfrac{1-\nu_{(j)}}{\rho^2} \\ 1+\nu_{(j)} & \dfrac{1-\nu_{(j)}}{\rho^2} \end{bmatrix} \begin{bmatrix} b^{(j)} \\ c^{(j)} \end{bmatrix}, \tag{22}$$

where

$$b^I = \frac{1}{\Delta}\Big\{ \left[(\kappa_3+\kappa_2)\,\eta_2{}^2 - \kappa_2 + \kappa_4\right]\eta_1\lambda + (\kappa_4+\kappa_3)\,\eta_2{}^2\Big\}, \tag{23a}$$

$$c^I = -\frac{1}{\Delta}\Big\{ \left[(\kappa_3-\kappa_1)\,\eta_2^2 + (\kappa_1+\kappa_4)\right]\eta_1\lambda + (\kappa_4+\kappa_3)\,\eta_1{}^2\Big\}\eta_2^2\,, \tag{23b}$$

$$b^{II} = \frac{1}{\Delta}\Big[(\kappa_2+\kappa_1)\,\eta_2^2\eta_1\lambda + (\kappa_2-\kappa_4)\,\eta_1^2 + (\kappa_1+\kappa_4)\,\eta_2^2\Big], \tag{23c}$$

$$c^{II} = -\frac{1}{\Delta}\Big[(\kappa_2+\kappa_1)\,\eta_1\lambda + (\kappa_3+\kappa_2)\,\eta_1^2 + (\kappa_1-\kappa_3)\,\eta_2^2\Big]\eta_2^2, \tag{23d}$$

and

$$\kappa_1 := \frac{\gamma}{1-\nu_1}, \quad \kappa_2 := \frac{\gamma}{1+\nu_1}, \quad \kappa_3 := \frac{1}{1-\nu_2}, \quad \kappa_4 := \frac{1}{1+\nu_2},$$
$$\Delta := \left[\kappa_2 - \kappa_4 - (\kappa_3+\kappa_2)\,\eta_2^2\right]\eta_1^2 + \left[(\kappa_3-\kappa_1)\,\eta_2^2 + \kappa_1 + \kappa_4\right]\eta_2^2.$$

By introducing $\xi := \eta_2/\eta_1 > 1$ it is a routine exercise to show that $\Delta = \eta_1^2\big[(\kappa_4+\kappa_3\eta_2^2)(\xi^2-1) + (\kappa_2+\kappa_1\xi^2)(1-\eta_2^2)\big] > 0$, so the expressions in (23) are well defined.

As for the out-of-plane displacement, w, from (15a) simple variational arguments lead to

$$D^{(j)}\nabla^4 w^{(j)} - \mathring{\boldsymbol{N}}^{(j)} : \left[\boldsymbol{\nabla}\otimes\boldsymbol{\nabla} w^{(j)}\right] = 0 \quad \text{in } \Omega_{(j)} \quad (j \in \{I, II\}). \tag{24}$$

Further rescaling,

$$w^{(j)} \to \frac{w^{(j)}}{h}, \qquad D^{(j)} \to \frac{h^2}{12U_2R_2} =: \mu^{-2}, \tag{25}$$

allows us to cast (24) in the dimensionless form

$$\mu^{-2}\nabla^4 w^{(j)} - \mathring{\sigma}_{rr}^{(j)}\frac{\partial^2 w^{(j)}}{\partial\rho^2} - \mathring{\sigma}_{\theta\theta}^{(j)}\frac{1}{\rho}\left[\frac{\partial w^{(j)}}{\partial\rho} + \frac{1}{\rho}\frac{\partial^2 w^{(j)}}{\partial\theta^2}\right] = 0. \tag{26}$$

Typically, μ^{-2} is a very small parameter ($0 < \mu^{-1} \ll 1$) for plates that are very thin or highly stretched (of course, within the limits of the theory employed herein).

The solution strategy for solving these equations mirrors closely the route pursued by Coman et al. [2, 3]. Looking for solutions with separable variables (the so-called *normal-mode approach*), we are prompted to consider

$$w^{(j)}(\rho,\theta) = W^{(j)}(\rho)\cos(n\theta), \quad (j \in \{I, II\}), \tag{27}$$

where $n \in \mathbb{N}$ represents the mode number (equal to half the number of regular wrinkles in the azimuthal direction), and the unknown amplitudes $W^{(j)}$ will be found by solving some simpler ordinary differential equations. We mention in passing that the mode number n must be the same in both Ω_I and Ω_{II} or otherwise discontinuities would arise between the wrinkled configurations of these two regions (hence, contradicting the perfect bond initially assumed to exist between these parts).

On substituting the ansatz (27) into (26), after eliminating the multiplicative common term $\cos n\theta$, we are left with solving two ordinary differential equations

$$\frac{d^4W^{(j)}}{d\rho^4} + \mathcal{C}_3^{(j)}(\rho)\frac{d^3W^{(j)}}{d\rho^3} + \mathcal{C}_2^{(j)}(\rho)\frac{\mathrm{d}^2W^{(j)}}{\mathrm{d}\rho^2} + \mathcal{C}_1^{(j)}(\rho)\frac{\mathrm{d}W^{(j)}}{\mathrm{d}\rho} + \mathcal{C}_0^{(j)}(\rho)W^{(j)} = 0, \quad \rho \in \Lambda_{(j)}, \tag{28}$$

where

$$\mathcal{C}_3^{(j)}(\rho) := \frac{2}{\rho}, \qquad \mathcal{C}_2^{(j)}(\rho) := -\left[\frac{2n^2+1}{\rho^2} + \mu^2\,\mathring{\sigma}_{rr}^{(j)}(\rho)\right],$$

$$\mathcal{C}_1^{(j)}(\rho) := \frac{1}{\rho}\left[\frac{2n^2+1}{\rho^2} - \mu^2\,\mathring{\sigma}_{\theta\theta}^{(j)}(\rho)\right], \quad \mathcal{C}_0^{(j)}(\rho) := \frac{n^2}{\rho^2}\left[\frac{n^2-4}{\rho^2} + \mu^2\,\mathring{\sigma}_{\theta\theta}^{(j)}(\rho)\right],$$

and $j \in \{I, II\}$. These two equations must be supplemented with appropriate boundary conditions. Using the rescaling and the normal mode approach introduced earlier on, the clamped boundary conditions at $\rho = \eta_1$ and $\rho = 1$ are simply

$$W^I(\eta_1) = \left.\frac{\mathrm{d}W^I}{\mathrm{d}\rho}\right|_{\rho=\eta_1} = 0 \quad \text{and} \quad W^{II}(1) = \left.\frac{\mathrm{d}W^{II}}{\mathrm{d}\rho}\right|_{\rho=1} = 0. \tag{29}$$

However, the continuity conditions along C_m demand a closer attention. First, let us note that kinematic considerations require that along the interface ($r = R_m$)

$$w^I = w^{II} \quad \text{and} \quad \nabla_r w^I = \nabla_r w^{II}. \tag{30}$$

This also implies that the variations of the out-of-plane displacements obey the same restrictions, i.e. $\delta w^I = \delta w^{II}$ and $\nabla_r(\delta w^I) = \nabla_r(\delta w^{II})$ along the interface. Second, if we apply (15b) to the entire bi-annular configuration, we get

$$\sum_{j=I,II}\int_{C_m}\Big\{ - D^{(j)}\boldsymbol{\nabla}(\nabla^2 w^{(j)}) - D^{(j)}(1-\nu_{(j)})\boldsymbol{\nabla}\cdot\big[(\boldsymbol{s}^{(j)}\otimes\boldsymbol{s}^{(j)})(\boldsymbol{\nabla}\otimes\boldsymbol{\nabla}w^{(j)})\big] + \mathring{\boldsymbol{N}}^{(j)}\cdot\boldsymbol{\nabla}w^{(j)}\Big\}\cdot\boldsymbol{n}^{(j)}\delta w^I\,\mathrm{d}S = 0, \tag{31}$$

where $j = I$ corresponds to the variables on the outer boundary of Ω_I, and $j = II$ is used for those associated with the inner boundary of Ω_{II}. In conclusion, since $\boldsymbol{n}^I = -\boldsymbol{n}^{II} = \boldsymbol{e}_r$, $\boldsymbol{s}^I = -\boldsymbol{s}^{II} = \boldsymbol{e}_\theta$ and $\delta w^I = \delta w^{II}$ is arbitrary, from (31) we deduce the interface constraint

$$D^I\big[\nabla_r(\nabla^2 w^I) + (1-\nu_1)\nabla_\theta(\nabla_{r\theta}w^I)\big] = D^{II}\big[\nabla_r(\nabla^2 w^{II}) + (1-\nu_2)\nabla_\theta(\nabla_{r\theta}w^{II})\big], \tag{32}$$

where use has been made of $\mathring{N}_{rr}^I(R_m) = \mathring{N}_{rr}^{II}(R_m)$ that follows from (20). We observe that (32) is the equilibrium of the vertical shear force resultants acting along the interface. Similar manipulations on (15c) eventually give another condition that needs to be satisfied along C_m, namely

$$D^I(\nabla_{rr}w^I + \nu_1\nabla_{\theta\theta}w^I) = D^{II}(\nabla_{rr}w^{II} + \nu_2\nabla_{\theta\theta}w^{II}); \tag{33}$$

this represents the equilibrium of bending moments along the interface. Analogous constraints were derived by Frostig and Simitses [4, 5], although in both of their works there appear to be some algebraic errors.

After using the rescaling introduced in (21) and employing the normal-mode approach (27), the kinematic continuity conditions (30) in conjunction with the natural constraints in (32) and (33) lead to the

non-dimensional matching equations at $\rho = \eta_2$

$$W^I = W^{II}, \tag{34a}$$

$$\frac{\mathrm{d}W^I}{\mathrm{d}\rho} = \frac{\mathrm{d}W^{II}}{\mathrm{d}\rho}, \tag{34b}$$

$$\beta_1\left(\frac{\mathrm{d}^2W^I}{\mathrm{d}\rho^2} + \frac{\nu_1}{\eta_2}\frac{\mathrm{d}W^I}{\mathrm{d}\rho} - \frac{\nu_1 n^2}{\eta_2^2}W^I\right) = \beta_2\left(\frac{\mathrm{d}^2W^{II}}{\mathrm{d}\rho^2} + \frac{\nu_2}{\eta_2}\frac{\mathrm{d}W^{II}}{\mathrm{d}\rho} - \frac{\nu_2 n^2}{\eta_2^2}W^{II}\right), \tag{34c}$$

$$\beta_1\left\{\frac{\mathrm{d}^3W^I}{\mathrm{d}\rho^3} + \frac{1}{\eta_2}\frac{\mathrm{d}^2W^I}{\mathrm{d}\rho^2} - \left[\frac{1+(2-\nu_1)n^2}{\eta_2^2}\right]\frac{\mathrm{d}W^I}{\mathrm{d}\rho} + \frac{(3-\nu_1)n^2}{\eta_2^3}W^I\right\}$$

$$= \beta_2\left\{\frac{\mathrm{d}^3W^{II}}{\mathrm{d}\rho^3} + \frac{1}{\eta_2}\frac{\mathrm{d}^2W^{II}}{\mathrm{d}\rho^2} - \left[\frac{1+(2-\nu_2)n^2}{\eta_2^2}\right]\frac{\mathrm{d}W^{II}}{\mathrm{d}\rho} + \frac{(3-\nu_2)n^2}{\eta_2^3}W^{II}\right\}, \tag{34d}$$

where

$$\beta_1 := \frac{\gamma}{1-\nu_1^2} \quad \text{and} \quad \beta_2 := \frac{1}{1-\nu_2^2}.$$

At this juncture some observations are appropriate. The eigenproblem describing the wrinkling bifurcations of the bi-annular plate has been cast in the form of a three-point boundary value problem for a fourth-order ordinary differential equation with variable coefficients. Note that although $\mathcal{C}_3^{(j)}$ and $\mathcal{C}_2^{(j)}$ are continuous, the other two coefficients, $\mathcal{C}_0^{(j)}$ and $\mathcal{C}_1^{(j)}$, are discontinuous. Owing to the presence of μ defined in (25), for thin plates ($\mu \gg 1$) this problem also displays a singular perturbation character: $\mu = \infty$ corresponds to the case of a radially stretched bi-annular *membrane* (no bending stiffness), which can be understood relatively easily as we show in the next section. When μ is large, but finite, it turns out that a change of tack is called for although, as it will be seen later in Section 4, the information obtained from the membrane case is still relevant for the clarification of that situation.

3. Basic state

Next, we are going to study the existence of compressive azimuthal stresses in Ω by using the expressions recorded in Equation (22), with an aim towards classifying some of the key features that are encountered for our particular loading conditions. A more comprehensive analytical study was undertaken by Coman [10], although the information we provide here is somewhat complementary to that study. For the sake of convenience, we introduce the terminology *'nodal hoop point'* (*NHP*) in relation to those values $\eta_1 \leq \bar{\rho} \leq 1$ for which $\mathring{\sigma}_{\theta\theta}(\bar{\rho}) = 0$.

In the case of the stretched homogeneous annulus discussed by Coman et al. [2, 3] there is at most one such *NHP* and the analysis is fairly straightforward. However, for a stretched bi-annular plate a routine (but tedious) analysis of Equation (22) reveals the possible existence of an additional *NHP*, and the situation is further complicated by having to account for the relative positions of these two points with respect to the boundaries C_j ($j = 1, 2$) and C_m.

Based on our extensive numerical simulations of the eigensystem consisting of (28), (29) and (34), we can classify the various situations encountered as shown in Table 1. The auxiliary notation introduced there stand for

$$I_a := \mathring{\sigma}^I_{\theta\theta}(\eta_1), \quad I_b := \mathring{\sigma}^I_{\theta\theta}(\eta_2), \tag{35a}$$

$$II_a := \mathring{\sigma}^{II}_{\theta\theta}(\eta_2), \quad II_b := \mathring{\sigma}^{II}_{\theta\theta}(1). \tag{35b}$$

(The reason we consider values of the pre-buckling azimuthal stresses on the two boundaries of Ω and along the interface is because these stresses are monotonic.)

Table 1. Classification of the pre-buckling azimuthal stresses $\mathring{\sigma}_{\theta\theta}(\rho)$ in the uniformly stretched bi-annular elastic plate; the notation $I_{a,b}, II_{a,b}$ are defined in (35). The black bullets on the dashed lines in each sketch identify the location of the *nodal hoop points* (*NHP*) $\eta_1 < \overline{\rho} < 1$ for which $\mathring{\sigma}_{\theta\theta}(\overline{\rho}) = 0$. The coloured markers indicate the colour-coding associated with the type of pre-buckling azimuthal stresses and are used later in Figures 3 and 4.

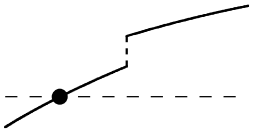	$\mathcal{B}_1$, 1*NHP* in Ω_I $I_a < 0 < I_b$, $II_a, II_b > 0$, and $I_b < II_a$	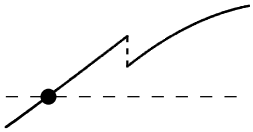	$\mathcal{B}_2$, 1*NHP* in Ω_I $I_a < 0 < I_b$, $II_a, II_b > 0$, and $I_b < II_a$
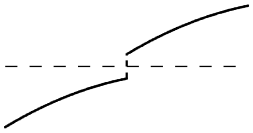	$\mathcal{K}$, 0*NHP* $I_a < I_b < 0$ and $0 < II_a < II_b$	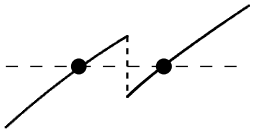	$\mathcal{R}$, 2*NHP* in $\Omega_{I,II}$ $I_a < 0 < I_b$ and $II_a < 0 < II_b$
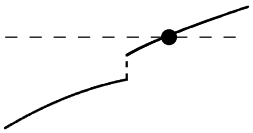	$\mathcal{G}_1$, 1*NHP* in Ω_{II} $II_a < 0 < II_b$ and $I_a < I_b < 0$	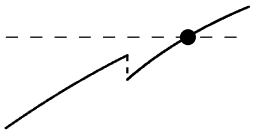	$\mathcal{G}_2$, 1*NHP* in Ω_{II} $I_a, I_b < 0$ and $II_a < 0 < II_b$
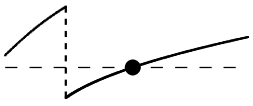	$\mathcal{Y}$, 1*NHP* in Ω_{II} $I_a, I_b > 0$ and $II_a < 0 < II_b$		

To get a better understanding of the role played by the theoretical scenarios summarized in Table 1, brute-force numerical simulations have been carried out to check the sign of the pre-buckling azimuthal stresses in Ω. For convenience, we plotted our results using the $\eta_1 - \lambda$ plane (this means that all of the other parameters were kept fixed). Figures 3 and 4 include the most representative behaviours of the azimuthal stresses; the background is coloured according to the conventions defined in Table 1. We draw the attention to the fact that, from the point of view of a pure membrane ($\mu = \infty$), as λ is progressively increased from zero, the onset of compressive stresses coincides with the instant when the value of this parameter first reaches the boundary separating the coloured background region from the white one. That curve can be regarded as the graph of a well-defined mapping $\eta_1 \to \lambda^{\text{low}}(\eta_1)$. With this convention in mind, the observation just made above indicates that wrinkling of the bi-annular membrane occurs as soon as $\lambda = \lambda^{\text{low}}$; for a plate, the counterpart of this statement would be $\lambda \geq \lambda^{\text{low}}$, i.e. we only get a lower bound (because a plate can support compressive stresses, unlike a membrane).

Some subtle properties of the mapping $\eta_1 \to \lambda^{\text{low}}(\eta_1)$ can be understood in analytical terms, as we now show. Note that, according to the representative sample of numerical results included in Figures 3 and 4, the graph of this mapping displays two distinct types of behaviour: one is characterized by a kink-like (non-convex) shape, always with the red ($\mathcal{R}$) and yellow ($\mathcal{Y}$) background regions invariably adjacent to each other; the other situation involves only monotonic behaviour, with the black ($\mathcal{K}$) region always positioned next to the light-blue ($\mathcal{B}_2$) or light-green ($\mathcal{G}_2$) parts.

Given the large number of non-dimensional parameters, see Equations (23), it would be of interest to have some clear criteria that discern between these two cases. To this end, let us consider the equation $I_a(\eta_1, \eta_2; \lambda) = 0$, that is to be solved for λ. It follows that

$$\lambda = \lambda_1^{\text{low}} := \frac{4\gamma\nu_1\eta_1\eta_2^2}{(1-\nu_1^2)(1-\nu_2^2)\left[\kappa_1(\kappa_2-\kappa_4-(\kappa_2+\kappa_3)\eta_2^2)\eta_1^2+\kappa_2(\kappa_1+\kappa_4-(\kappa_1-\kappa_3)\eta_2^2)\eta_2^2\right]},$$

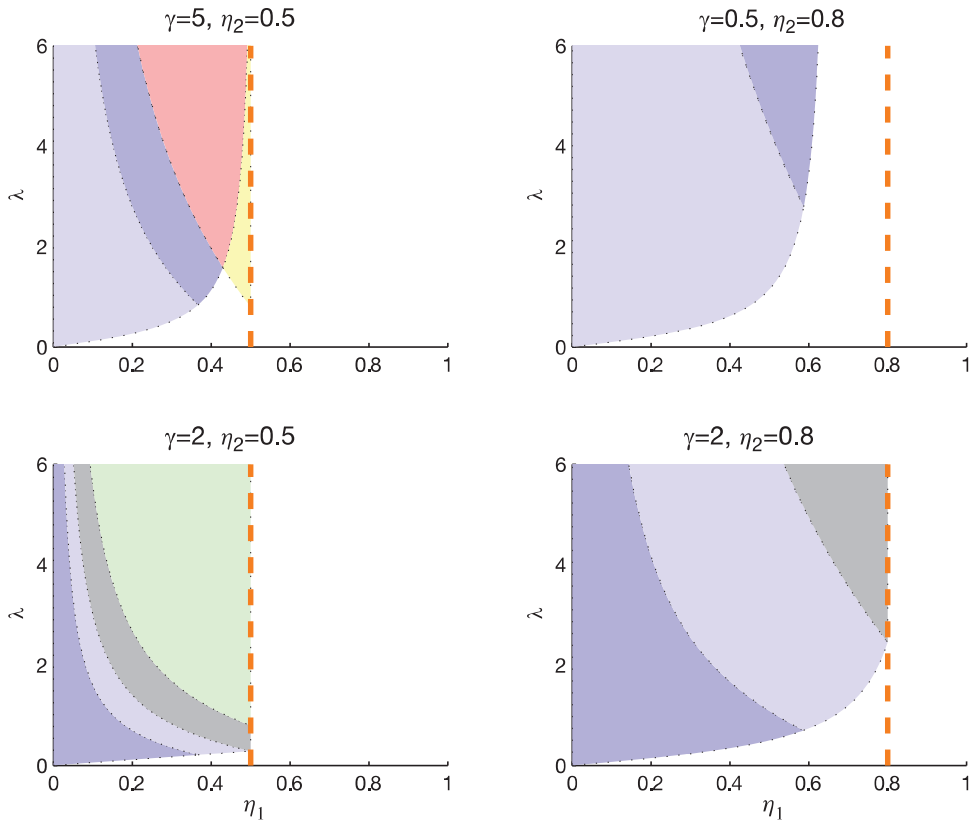

Figure 3. Characterization of the pre-buckling azimuthal stresses following the conventions outlined in Table 1. In all plots $\nu_1 = \nu_2 = 0.3$, while γ and η_2 take the values recorded in the individual titles.

which always passes through the origin $(0, 0)$ of the λ–η_1 plane. A lengthy (but routine) analysis also demonstrates that λ_1^{low} is always positive before the denominator of the above expression changes sign from positive to negative. Furthermore, $\lambda_1^{\text{low}} \to \infty$ for

$$\eta_1 = \eta_2 \sqrt{\frac{(1-\nu_2)\left[1-\nu_1+\gamma(1+\nu_2)\right]+(1+\nu_2)\left[1-\nu_1-\gamma(1-\nu_2)\right]\eta_2^2}{(1-\nu_2)\left[1+\nu_1-\gamma(1+\nu_2)\right]+(1+\nu_2)\left[1+\nu_1+\gamma(1-\nu_2)\right]\eta_2^2}},$$

provided that the coefficient of η_2 above falls between 0 and 1, that is

$$\eta_2 > \sqrt{\left(\frac{1-\nu_2}{1+\nu_2}\right)\cdot\frac{\gamma(1+\nu_2)-\nu_1}{\gamma(1+\nu_2)+\nu_1}} := \bar{\eta}_2.$$

As a matter of fact, in Figures 3 and 4 this λ_1^{low} provides the boundary between the bottom-side white region and the blue regions $\mathcal{B}_{1,2}$. Moreover, in the case characterized by the presence of the "kink", it also acts as the bounding curve between the red ($\mathcal{R}$) and yellow ($\mathcal{Y}$) regions.

Similarly, if we solve for λ in $II_a(\eta_1, \eta_2; \lambda) = 0$ we find

$$\lambda = \lambda_2^{\text{low}} := \left(\frac{1-\nu_1^2}{1-\nu_2^2}\right)\cdot\frac{(1+\nu_1)(1-\nu_1+\gamma\nu_2)\eta_2^2-(1-\nu_1)(1+\nu_1-\gamma\nu_2)\eta_1^2}{\gamma\eta_1\left[1-\nu_2-(1+\nu_2)\eta_2^2\right]},$$

which gives the bound between the red ($\mathcal{R}$) and blue ($\mathcal{B}_1$) regions. Thus, the values of $\eta_1 \in (0, \eta_2)$ that are compatible with the existence of the "kink" are expected to satisfy $I_a = II_a = 0$ simultaneously. Solving

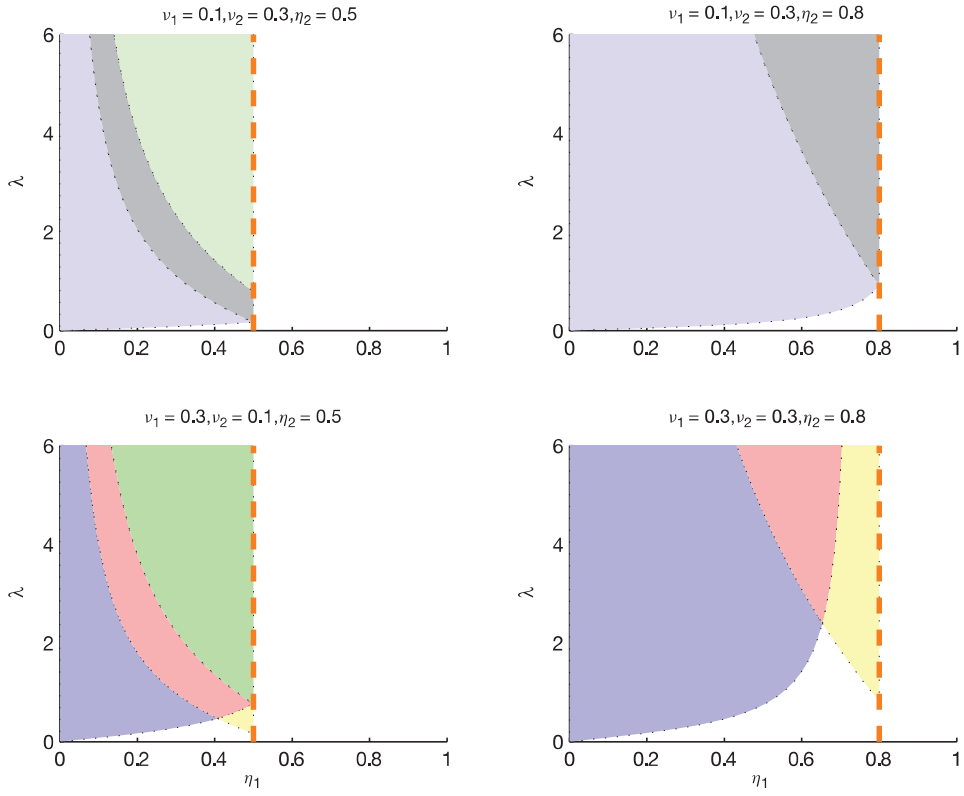

Figure 4. As per Figure 3 except for $\gamma = 1$ in all subplots.

$\lambda_1^{\text{low}}(\eta_1) = \lambda_2^{\text{low}}(\eta_1)$ and discarding the invalid roots η_1, we are left with the value

$$\eta_1^{\text{kink}} = \eta_2 \sqrt{\frac{1 - \nu_1 + \gamma \nu_2}{1 + \nu_1 - \gamma \nu_2}}. \tag{36}$$

This represents the abscissa of the "kink" and we note that, *a priori*, the value provided by (36) need not be situated within the appropriate range. Thus, the possibility of having a "kink" is guaranteed by demanding that $0 < \eta_1^{\text{kink}} < \eta_2$, which in turn requires $0 < \gamma < \nu_1/\nu_2$. On the other hand, if $\gamma > \nu_1/\nu_2$ then η_1^{kink} falls outside $(0, \eta_2)$ and the graph of $\lambda^{\text{low}}(\eta_1)$ has a monotonic shape. In conclusion, we can make the following important observations

$$\eta_1 \to \lambda^{\text{low}}(\eta_1) : \begin{cases} \text{kinked-shape} & \text{if } 0 < \gamma < \nu_1/\nu_2, \\ \text{monotonic-shape} & \text{if } \gamma > \nu_1/\nu_2. \end{cases} \tag{37}$$

It is interesting to mention in passing that if $\nu_1 > \nu_2$, then the "kink" will be present when $0 < \gamma < 1$, a result that was already anticipated by an earlier analysis of Coman [10]. However, the precise criteria spelled out in (37) significantly improve upon the earlier observations.

4. Wrinkling problem

The numerical integration of the eigensystem consisting of (28), (29) and (34) can be executed by using several different strategies. One of the non-trivial features is the presence of the interface requiring the solutions of (28) to be matched via the Equations (34); in standard terminology, we are dealing here with a three-point boundary-value problem. One possible option is to use the MATLAB software 'sbvp' (see [15, 16]), which displays a robust performance in a variety of contexts, including nonlinear eigen-problems [17]. By using a standard transformation (e.g. see [18]) the fourth-order three-point eigenproblem can be re-written as a nonlinear eighth-order one; both the eigenvalues and the corresponding eigenmodes are then readily available. Other alternatives

are the *finite-difference method* [8] and a version of the *compound matrix method* described by Lindsay [19]. The disadvantage of the latter option consists in the fact that only the eigenvalues are available; to get the eigenmodes one must turn to standard boundary-value solvers such as those already mentioned above. We have used all three approaches to check the accuracy of our results. A further check was performed by letting $\gamma = 1$, $\nu_1 = \nu_2$ and considering various choices for η_1 and η_2. The results were then compared with those obtained in the case of a simple annular plate having uniform material properties (Coman and Haughton [2]).

4.1. Individual response curves

Although the analysis of the basic state presented in Section 3 gives a rough idea of some characteristics for the possible wrinkling instabilities experienced by the bi-annular plate, it is insufficient by itself if we assume that the non-dimensional bending stiffness μ is finite. In this case we must turn to the individual *response curves* $\lambda = \lambda(\eta_1; \eta_2, \mu, n, \gamma, \nu_1, \nu_2)$; here, the eigenvalue ($\lambda$) is regarded as a function of η_1, with all of the other parameters being kept fixed. The dependence on $n \in \mathbb{N}$ is particularly important and that is why, for future reference, we are going to label these curves as $C^{(n)}$. Recall that the mode number $n \in \mathbb{N}$ was artificially introduced in the problem through the separable-variable solution (27) so, eventually, we need to identify those values which lead to the smallest eigenvalue. It is for this reason that the individual response curves need to be plotted for a whole range of mode numbers. A similar approach was taken in the earlier work of the first author, to which the interested reader is referred for more details.

The relevant numerical results are recorded in Figures 5 and 6. In each set of plots there are two families of curves $C^{(n)}$ shown in different colours. The red ones are obtained by using $n \ll \mu^{1/2}$, and they correspond (roughly) to the membrane-like regime identified by Coman and Haughton [2]. This behaviour contributes nothing to the neutral stability envelope even though, unlike in the reference just cited, the dependence λ versus η_1 is not always monotonic; see Figure 5. However, it is still true that $C^{(n)}$ is always situated above $C^{(n+1)}$ for the entire range of relevant values $\eta_1 \in (0, \eta_2) \subset (0, 1)$, and for this particular reason we keep the same terminology.

The other set of curves, shown in blue, and for which $\mathcal{O}(\mu^{1/2}) \leq n \ll \mathcal{O}(\mu)$, are basically the building blocks of the neutral stability envelope. In the language of [2] this will form the plate-like regime although, again, that terminology is not strictly applicable here because in some cases these curves are "kinked". The existence of this feature can be traced back to the basic state. It was pointed out in Section 3 that the existence of compressive stresses in the membrane case ($\mu = \infty$) requires $\lambda \geq \lambda^{\text{low}}$. This λ^{low} was a non-smooth function of η_1 that had a discontinuous derivative at $\eta_1 = \eta_1^{\text{kink}}$. The blue curves in Figures 5 have a similar shape, except that the "kink" is smooth (no derivative discontinuities). However, as $\mu \to \infty$ the envelope of the individual response curves approaches the graph of $\eta_1 \to \lambda^{\text{low}}(\eta_1)$. The neutral stability envelope is discussed in more detail in the next section (also, see the recent study by one of us [10] that touches on several aspects on which we do not dwell here). Figure 6 contains information pertaining to the case when the neutral stability curves do not have any "kink" (see the discussion in Section 3), a case which otherwise is identical to what has already been said above.

4.2. Critical wrinkling modes

We are now in position to investigate the role played by the mechanical parameters $\gamma \equiv E_1/E_2$, ν_1 and ν_2 on the *neutral stability curves*. Here, these curves are defined as the graphs of the mapping $\eta_1 \to \lambda_C(\eta_1) := \min_{n \in \mathbb{N}} \lambda(\eta_1; n)$; the value of $n \in \mathbb{N}$ for which this minimum is attained represents the *critical mode number* and will be denoted by n_C henceforth. In adopting this particular definition for λ_C it is tacitly assumed that all of the other parameters are kept fixed (in particular, the location of the interface, η_2).

Our main priority is to shed some light on the buckling strength of the bi-annular configuration as compared to the simple annulus discussed by Coman and Haughton [2]. A first set of numerical results is included in Figure 7, which corresponds to an interface placed at $\eta_2 = 0.5$ with $\nu_1 = \nu_2 = 0.3$. On the left, the red continuous curve represents λ_C for a simple annular plate ($\gamma = 1$), while the other two sets of results in the same window correspond to $1 > \gamma = 0.5$ and $1 < \gamma = 2$. Rather unexpectedly, in the former case the critical eigenvalues are always above the red curve, indicating that plates with $E_1 < E_2$ offer more resistance to tensile wrinkling instabilities. The critical mode numbers shown in the right window display similar tendencies, but as η_1 gets closer to η_2 the pattern is somewhat reversed. Another interesting feature is that in the limit $\eta_1 = \eta_2$ all three sets of curves in both windows seem to converge to the same point. In this case the inner annulus "disappears" and the bi-annular plate degenerates into a simple annulus of inner radius η_2 and outer radius 1.

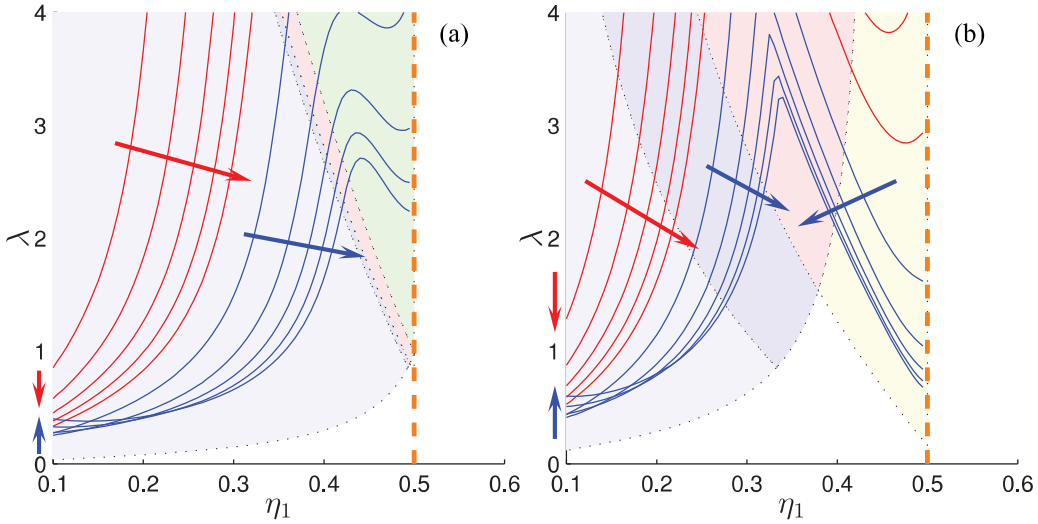

Figure 5. Dependence of the eigenvalue λ on the parameter η_1 for $\mu = 400.0, \gamma := E_1/E_2 = 0.3$, with the locations of the interface at $\eta_2 = 0.5$ (the vertical dashed line). The values of the mode number are $n = 6, 8, 10, 12, 14$ (*red curves*) and $20, 30, 40, 50, 60, 70$ (*blue curves*). In (a), $\nu_1 = 0.1,\ \nu_2 = 0.3$, while in (b), $\nu_1 = 0.3,\ \nu_2 = 0.1$. The arrows indicate the direction of increase for the mode number n, and the colour background shows the classification of the pre-buckling azimuthal stresses introduced in Table 1.

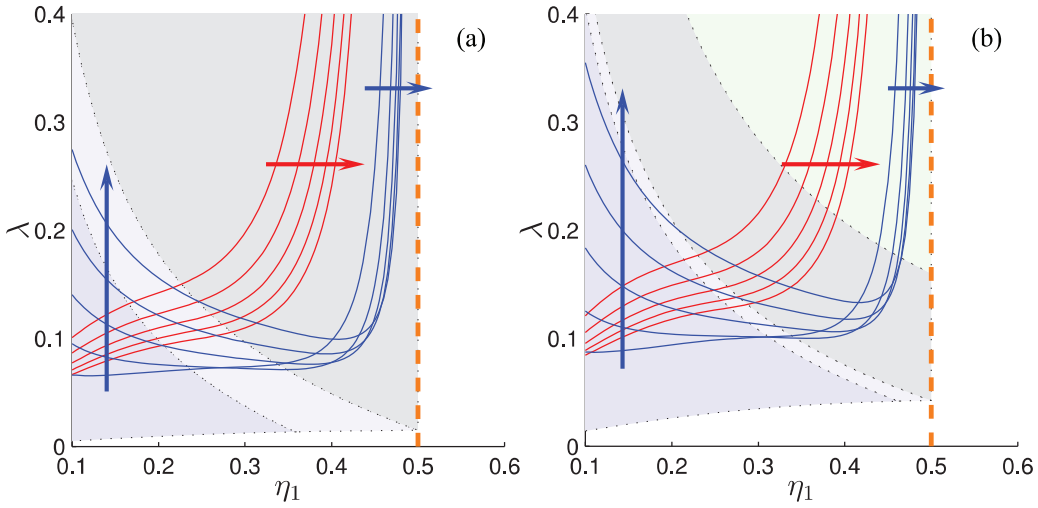

Figure 6. Dependence of the eigenvalue λ on the parameter η_1 for $\mu = 400.0, \gamma := E_1/E_2 = 10.0$; everything else is as in Figure 5.

Extensive numerical experiments, not shown here because of a lack of space, indicated that these phenomena are robust and are encountered for other values of γ and ν_j $(j = 1, 2)$.

It is also of interest to investigate the role of the Poisson's ratios ν_1 and ν_2 on the behaviour of λ_C when γ is kept fixed. The notation $\lambda_C = \lambda_C(\nu_1, \nu_2)$ will be used for denoting the critical eigenvalues (or the neutral stability envelope) for a bi-annular plate with Poisson's ratios ν_1 and ν_2 for Ω_I and Ω_{II}, respectively. A representative sample of results is recorded in Figure 8, where we take $\gamma = 1$. Looking at the sets of plots in the left window it is seen that if $\nu_1 > \nu_2$ (yellow markers) the corresponding neutral stability envelope $\lambda_C(\nu_1, \nu_2)$ is always below that associated with an annular plate of Poisson's ratio ν_1 (red curve). At the same time, this curve is above the blue one, which shows λ_C for an annular plate with $\nu = \nu_2$. If $\nu_1 < \nu_2$ the situation is exactly the opposite. It is apparent from Figure 8(a) that $\lambda_C(\nu_1, \nu_1)$ and $\lambda_C(\nu_2, \nu_2)$ serve as lower and upper bounds for $\lambda_C(\nu_1, \nu_2)$ and $\lambda_C(\nu_2, \nu_1)$ when $\gamma \equiv E_1/E_2$ is held fixed (this property was checked for a whole range of other values of γ). The trends exhibited by the critical mode numbers are shown in Figure 8(b).

As anticipated by the direct numerical simulations of the response curves in Section 4.1, and confirmed by the results shown in Figures 7 and 8, the neutral stability curves $\eta_1 \to \lambda_C(\eta_1)$ fall into two broad classes. One of

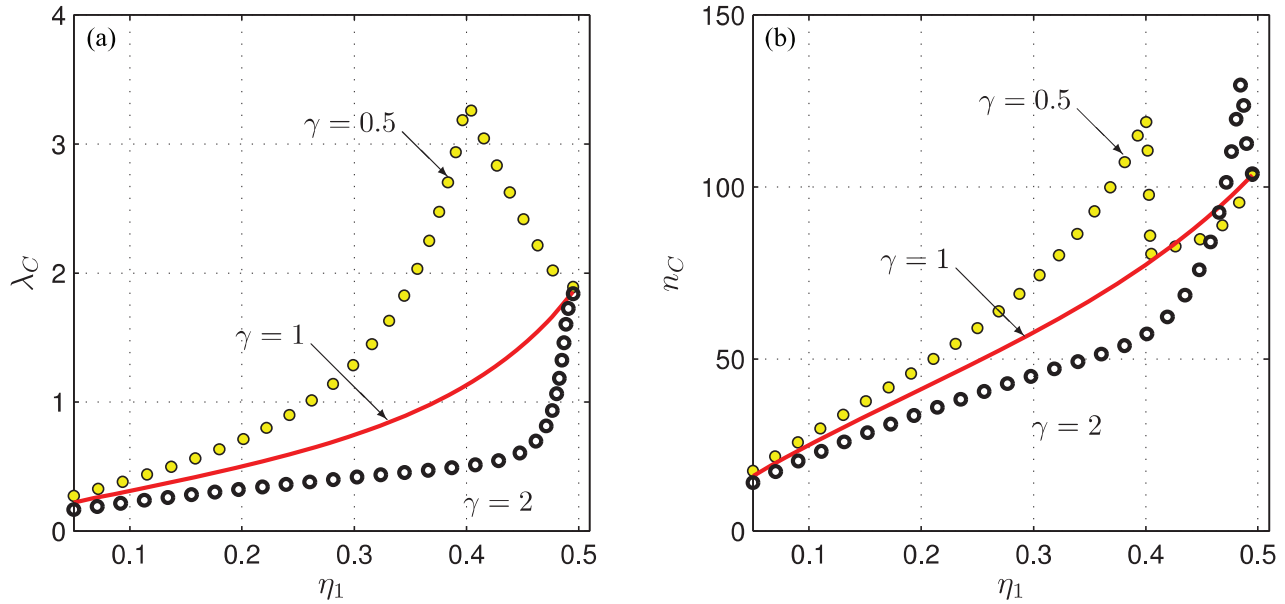

Figure 7. Dependence of the critical eigenvalues λ_C and the corresponding critical mode number n_C on the ratio of the Young's moduli of the two annular sub-regions, $\gamma := E_1/E_2$. Here we take $\nu = 400$, $\nu_1 = \nu_2 = 0.3$ and $\eta_2 = 0.5$.

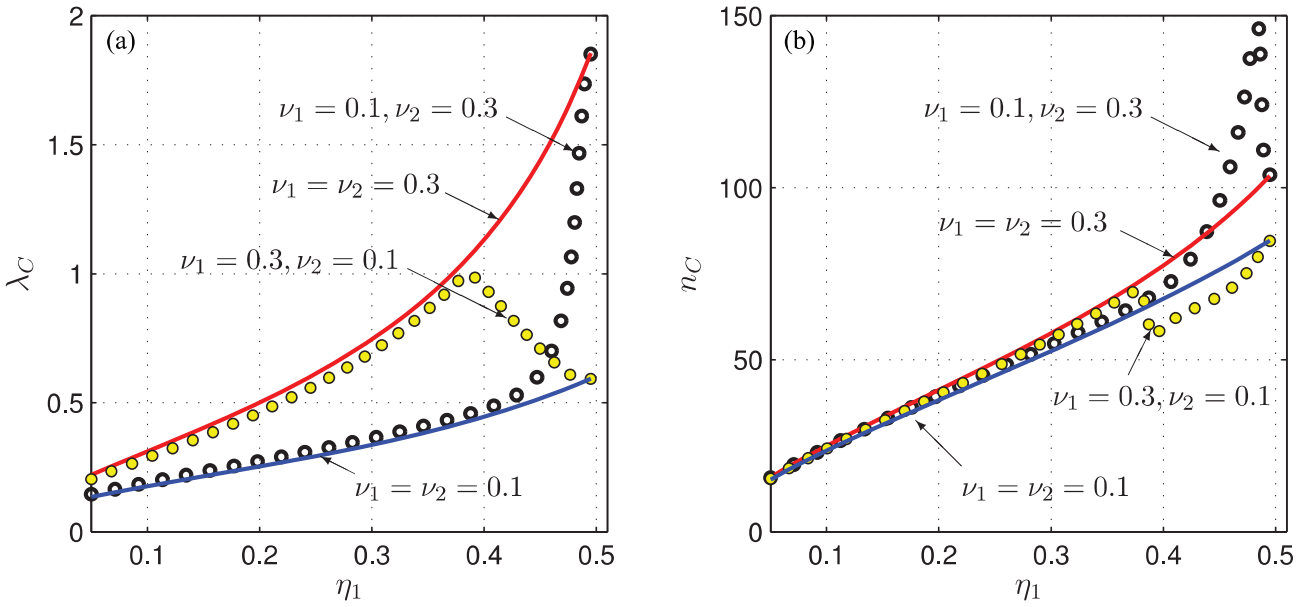

Figure 8. Dependence of the critical eigenvalues λ_C and the corresponding critical mode number on the ratio of Poisson ratio of two annuli ν_1/ν_2, other parameters are adopted as $\nu = 400$, $\gamma := E_1/E_2 = 1$ and $\eta_2 = 0.5$.

them is characterized by the non-convex (kink-like) shape seen in the curves represented with yellow markers in the aforementioned set of plots; the other class consists of a monotonic shape that gets steeper and steeper as $\eta_1 \to \eta_2$ (white markers, same Figures). In light of our discussion of the basic state and λ^{low} in Section 3, this is not entirely unexpected because $\lambda_C \simeq \lambda^{\text{low}}$ as $\mu \gg 1$. We mention in passing that the role of the *NHP*s in the membrane case ($\mu = \infty$) is replaced by that of certain turning points in a couple of second-order ordinary differential equations that will be discussed in Section 5. In the meantime, a deeper understanding of the differences between the two possible occurrences will be achieved by examining what happens to the *critical* eigenmodes as $\eta_1 \to \eta_2$ in either case.

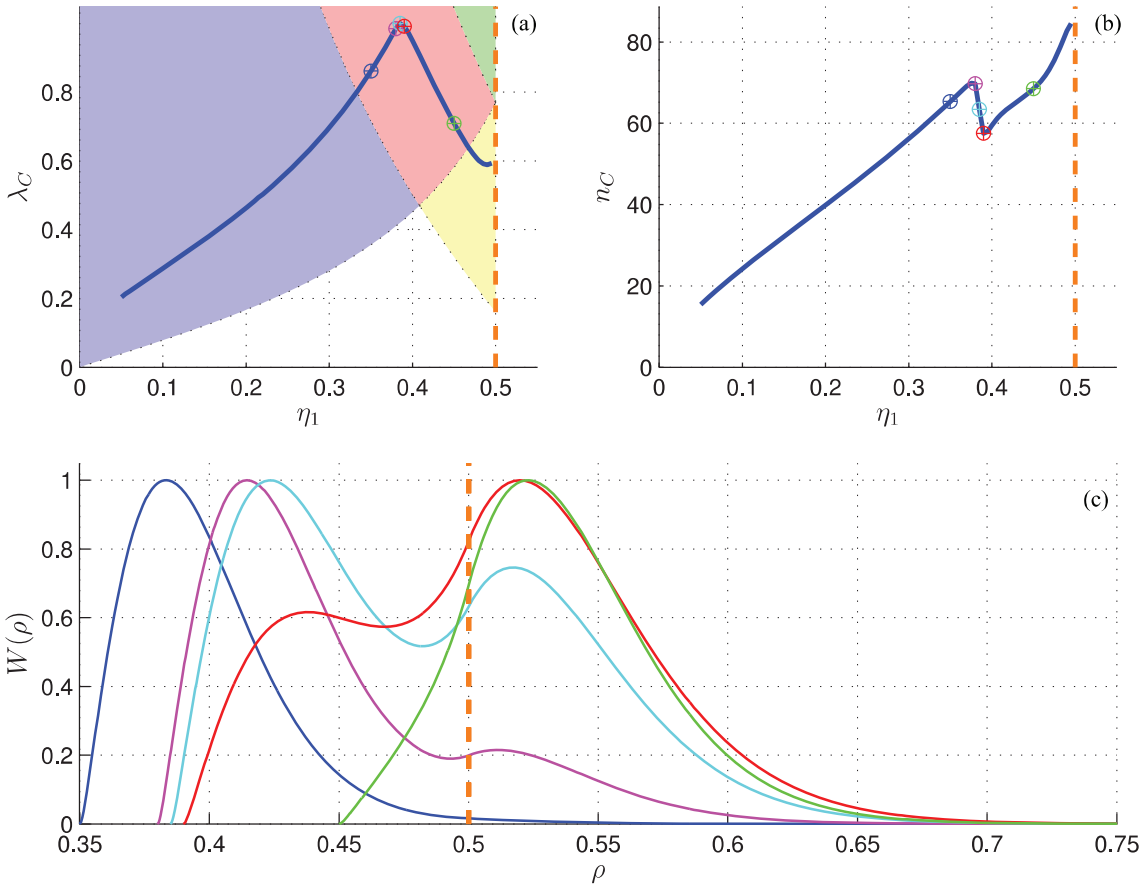

Figure 9. Morphological changes of the critical eigenmodes as $\eta_1 \to \eta_2$ before and after the "kink" in the neutral stability curves. In (a), the background colour indicates the classification of the pre-buckling azimuthal stresses that was introduced in Section 3. In both (a) and (b) we use different colours for $\oplus$ to show a sample of critical values of λ_C and n_C near the "kink", while in (c) the corresponding critical eigenmodes record the morphological changes seen in the radial direction of the bi-annular plate. Here $\mu = 400.0$, $\gamma = 1$, $\nu_1 = 0.3$, $\nu_2 = 0.1$ and $\eta_2 = 0.5$. From left to right, the eigenmodes correspond to $\eta_1 = 0.35, 0.38, 0.385, 0.39, 0.45$.

The first class of neutral stability curves (kink-type) is obtained for plates whose elastic constants satisfy $0 < \gamma < \nu_1/\nu_2$ – see Figure 9(a). Numerical experiments have revealed that when η_1 is to the left of the "kink" abscissa and $|\eta_1 - \eta_2| \simeq \mathcal{O}(1)$ then the critical eigenmodes are localized near the inner rim in Ω_I. As η_1 "moves" on the other side of the "kink", but far from it (i.e., $|\eta_1 - \eta_2| \ll 1$), the out-of-plane deformation is localized near the interface and confined entirely within Ω_{II}. Between these two extremes, there is an intermediate transition involving both sets of eigenmodes, and this is typically encountered in the vicinity of the "kink".

In Figure 9(a) and (b), we use the coloured markers $\oplus$ to locate the values of λ_C and n_C for an increasing set of values of η_1; the corresponding critical eigenmodes are shown with the same colour in Figure 9(c). The set of intermediate eigenmodes can be seen between the first (blue) and last (green) curves. With the largest amplitude normalized to be equal to 1, the localized part in Ω_I shrinks gradually as η_1 approaches the "kink" while, at the same time, there is a bump increase in Ω_{II} near the interface. When η_1 is sufficiently close to the "kink", the amplitudes of the wrinkles in both regions are of the same order. Note that n_C reaches its maximum at the "kink", and at this stage both sub-annular regions of the bi-annular plate experience wrinkling (while in Ω_{II} these wrinkles are localized near C_m, in Ω_I they have a rather diffuse character). As η_1 moves past the abscissa of the "kink", the bump in Ω_{II} enlarges with the decrease of that in Ω_I, and these changes are accompanied by a decrease in λ_C. The behaviour of n_C is slightly more exotic: at the "kink" the mode number starts to decrease for a very limited η_1 range and then continues to increase monotonically as $\eta_1 \to \eta_2$. It is worth pointing out that this type of transition occurs only in those cases in which the basic state has *NHP*'s in both sub-annular regions.

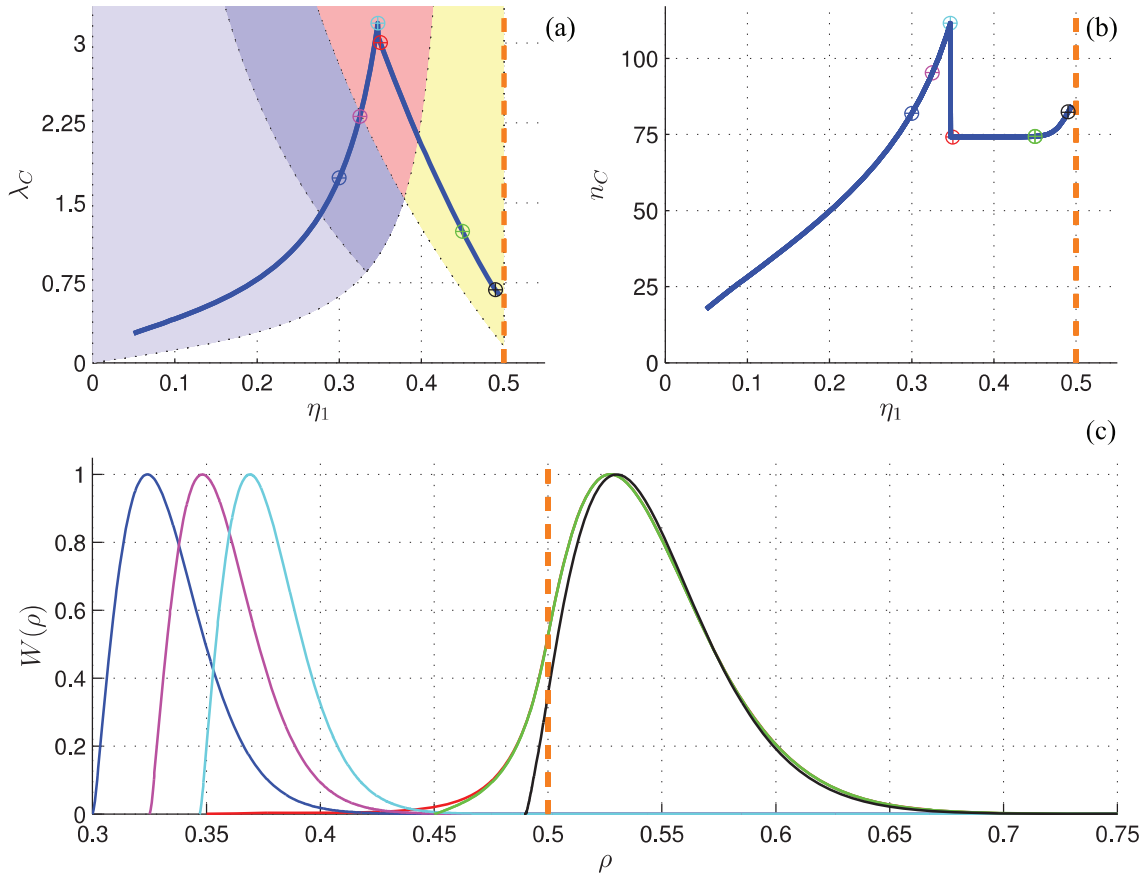

Figure 10. Same as Figure 9, except that here $\mu = 400.0$, $\gamma = 1$, $\nu_1 = 0.3$, $\nu_2 = 0.1$ and $\eta_2 = 0.5$. From left to right, the eigenmodes correspond to $\eta_1 = 0.35, 0.38, 0.385, 0.39, 0.45$.

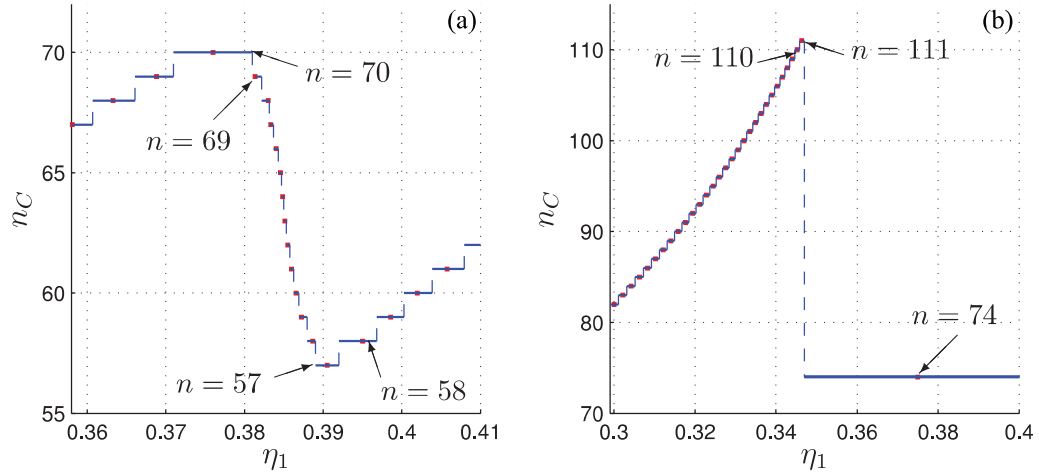

Figure 11. Enlarged view of the "kink" in the plots of n_C shown in Figures 9(b) and 10(b). For clarity, here we choose to emphasize the true piecewise-constant nature of the critical mode numbers.

Figure 10 shows another example of "kinked" neutral stability curves, which is characterized by a more pronounced sharpness. Now the behaviour of n_C and the sequence of changes undergone by the eigenmodes as $\eta_1 \to \eta_2$ is somewhat different: this is the situation analysed in detail by Coman in [10]. Further information regarding the nature of the critical mode numbers in the two cases just discussed above is included in Figure 11. Both windows in that figure emphasize the piecewise constant nature of n_C, and are obtained by zooming in the

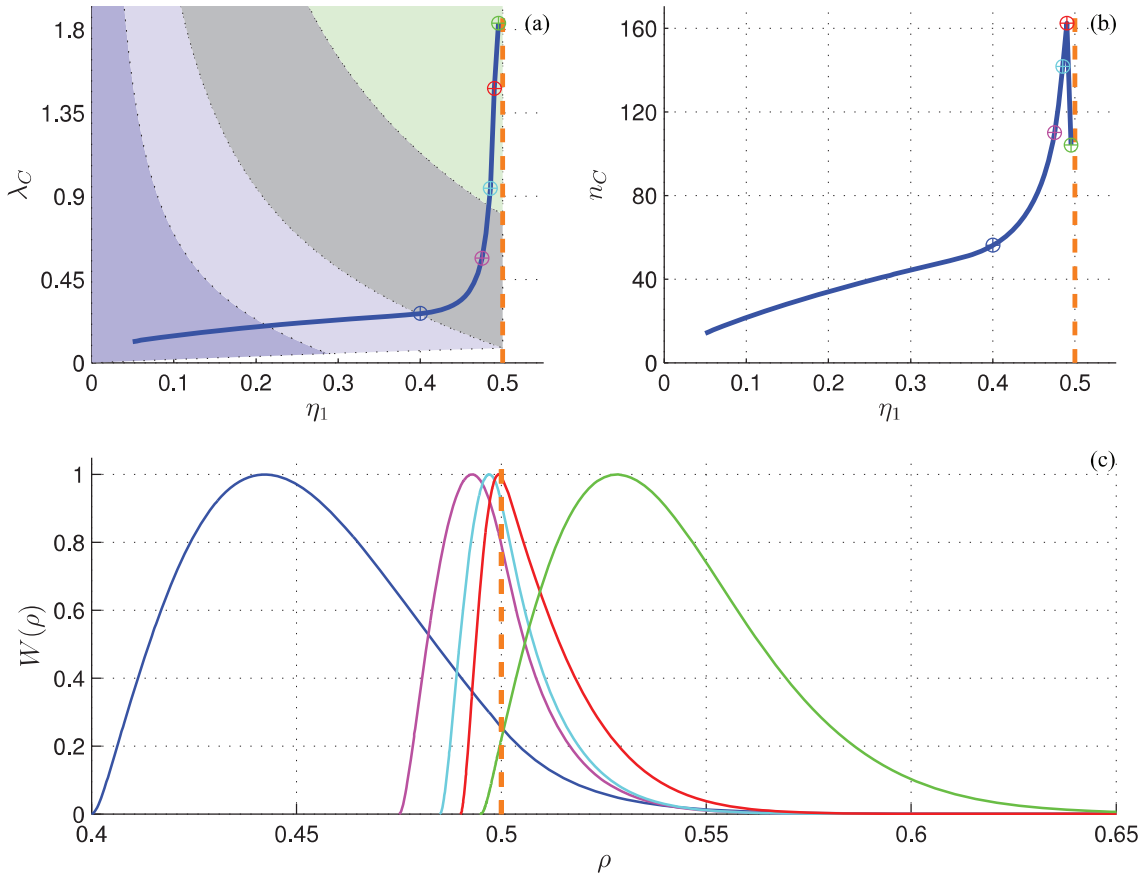

Figure 12. Morphological changes of the critical eigenmodes as $\eta_1 \to \eta_2$ for the monotonic-type neutral stability curves. The subplots are similar to those seen in Figure 10, but $\mu = 400.0$, $\gamma = 2$, $\nu_1 = 0.1$, $\nu_2 = 0.3$ and $\eta_2 = 0.5$. From left to right the eigenmodes shown correspond to $\eta_1 = 0.4, 0.475, 0.485, 0.49, 0.495$.

regions around the kinks in Figures 9(b) and 10(b). (Note that, by necessity, in the numerical simulations one has to regard the mode number n as a real variable, whereas in reality this is supposed to be a natural number.)

The existence of the second class of neutral stability curves (monotonic-type) is intimately connected to similar behaviour in $\eta_1 \to \lambda^{\text{low}}(\eta_1)$, as documented in Section 3. Details of this scenario are included in Figure 12. Let us note that, even though such curves resemble closely those for the stretched simple annular plate of Coman and Haughton [2], there are some subtle differences that are not immediately obvious. For example, in the case of a bi-annular plate $\lambda_C(\eta_1)$ is very small when $|\eta_1 - \eta_2| \simeq \mathcal{O}(1)$ and there is a very sharp increase in the critical eigenvalues as $\eta_1 \to \eta_2$, although this limit does not lead to a true blow-up behaviour as in the related works by Coman et al. [20, 21].

Some of these unusual properties can be understood further by looking at the critical eigenmodes. For configurations in which the inner rim is sufficiently far apart from the interface, these functions are localized entirely within Ω_I. As the breadth of this inner annular region decreases, the eigenmodes seem to undergo a shift to the right, without any significant changes in their qualitative properties; when $\eta_1 \simeq \eta_2$ the wrinkling is localized in Ω_{II} near the interface. It is interesting to mention that as the wrinkles "move" towards the interface, both λ_C and n_C increase sharply. As the wrinkles crest crosses the interface, n_C arrives at its maximum value, and after that it starts dropping down until a final finite value is reached (corresponding to $\eta_1 = \eta_2$). During the full range of the entire transition the critical mode has just one bump.

5. Asymptotic reduction

Additional numerical simulations (not shown here) have predicted that the critical mode number grows with μ, suggesting that in the limit of interest (very thin plates) both $\mu \gg 1$ and $n \gg 1$. This opens the possibility of an

asymptotic simplification for the complicated equations describing the wrinkling bifurcations of the bi-annular configuration.

The analysis of this section represents a non-trivial extension of the method proposed by Coman and Haughton [2]. By using similar arguments as in that reference, when $1 \ll n \ll \mu$ the original equations (28) can be reduced to

$$\frac{\mathrm{d}^2\overline{W}^{(j)}}{\mathrm{d}\rho^2} + \frac{1}{\rho}\left[\frac{\mathring{\sigma}^{(j)}_{\theta\theta}(\rho)}{\mathring{\sigma}^{(j)}_{rr}(\rho)}\right]\frac{\mathrm{d}\overline{W}^{(j)}}{\mathrm{d}\rho} - \frac{n^2}{\rho^2}\left[\left(\frac{n}{\mu}\right)^2\frac{1}{\rho^2\mathring{\sigma}^{(j)}_{rr}(\rho)} + \frac{\mathring{\sigma}^{(j)}_{\theta\theta}(\rho)}{\mathring{\sigma}^{(j)}_{rr}(\rho)}\right]\overline{W}^{(j)} = 0, \quad (j \in \{I, II\}), \tag{38}$$

but at this stage we leave open whether $n \ll \mathcal{O}(\mu^{1/2})$, $n = \mathcal{O}(\mu^{1/2})$ or $n \gg \mathcal{O}(\mu^{1/2})$. (It was discovered that the simplified equations recorded above, when solved subject to appropriate boundary and matching conditions, are capable of reproducing both the membrane- and plate-like regimes hinted at in Section 4.1.)

Since the order of our three-point boundary-value problem has decreased from 4 to 2, we are left with the task of identifying the reduced versions of the boundary constraints (29) and the interfacial conditions (34). As the original differential equations in both Ω_I and Ω_{II} are of the fourth-order, the functions $W^{(j)}(\rho)$ can be represented as linear combinations of four of linearly independent solutions of (28), i.e.

$$W^{(j)}(\rho) = \sum_{i=1}^{4} C_i^{(j)} W_i^{(j)}(\rho), \quad (j \in \{I, II\}), \tag{39}$$

where $C_i^{(j)} \in \mathbb{R}$ $(i = 1, \ldots, 4)$ denote eight constants that are to be determined by applying the four boundary constraints (29) together with the four continuity conditions (34). Following this strategy we end up with a homogeneous eighth-order linear algebraic system for $C_i^{(j)}$ whose nontrivial solvability requires that the determinant of the coefficient matrix, $\mathcal{D}(\lambda; \mu, \nu_1, \nu_2, \eta_1, \eta_2, n)$ (say), vanishes. The derivation of the relevant arguments is fairly involved and requires the introduction of additional notations. The boundary conditions (34) can be cast in matrix form by introducing

$$\boldsymbol{y}^{(j)} := \left[W^{(j)}, \frac{\mathrm{d}W^{(j)}}{\mathrm{d}\rho}, \frac{\mathrm{d}^2W^{(j)}}{\mathrm{d}\rho^2}, \frac{\mathrm{d}^3W^{(j)}}{\mathrm{d}\rho^3}\right]^{\mathrm{T}},$$

so that

$$\boldsymbol{G}\boldsymbol{y}^{I}(\eta_2) - \boldsymbol{H}\boldsymbol{y}^{II}(\eta_2) = \boldsymbol{0}. \tag{40}$$

The nonzero elements of the matrices $\boldsymbol{G} = (G_{ij})$ and $\boldsymbol{H} = (H_{ij})$ are

$$G_{11} = G_{22} = 1, \quad H_{11} = H_{22} = 1,$$

$$G_{31} = -\beta_1\frac{n^2\nu_1}{\eta_2^2}, \quad G_{32} = \beta_1\frac{\nu_1}{\eta_2}, \quad G_{33} = \beta_1,$$

$$H_{31} = -\beta_2\frac{n^2\nu_2}{\eta_2^2}, \quad H_{32} = \beta_2\frac{\nu_2}{\eta_2}, \quad H_{33} = \beta_2,$$

$$G_{41} = \frac{\beta_1}{\eta_2^3}(3-\nu_1)n^2, \quad G_{42} = -\frac{\beta_1}{\eta_2^2}\left[1+(2-\nu_1)n^2\right], \quad G_{43} = \frac{\beta_1}{\eta_2}, \quad G_{44} = \beta_1,$$

$$H_{41} = \frac{\beta_2}{\eta_2^3}(3-\nu_2)n^2, \quad H_{42} = -\frac{\beta_2}{\eta_2^2}\left[1+(2-\nu_2)n^2\right], \quad H_{43} = \frac{\beta_2}{\eta_2}, \quad H_{44} = \beta_2,$$

The determinant equation can be shown to be

$$\begin{vmatrix} W_1^I(\eta_1) & W_2^I(\eta_1) & W_3^I(\eta_1) & W_4^I(\eta_1) & 0 & 0 & 0 & 0 \\ W_1^{I'}(\eta_1) & W_2^{I'}(\eta_1) & W_3^{I'}(\eta_1) & W_4^{I'}(\eta_1) & 0 & 0 & 0 & 0 \\ \mathcal{D}_{31} & \mathcal{D}_{32} & \mathcal{D}_{33} & \mathcal{D}_{34} & \mathcal{D}_{35} & \mathcal{D}_{36} & \mathcal{D}_{37} & \mathcal{D}_{38} \\ \mathcal{D}_{41} & \mathcal{D}_{42} & \mathcal{D}_{43} & \mathcal{D}_{44} & \mathcal{D}_{45} & \mathcal{D}_{46} & \mathcal{D}_{47} & \mathcal{D}_{48} \\ \mathcal{D}_{51} & \mathcal{D}_{52} & \mathcal{D}_{53} & \mathcal{D}_{54} & \mathcal{D}_{55} & \mathcal{D}_{56} & \mathcal{D}_{57} & \mathcal{D}_{58} \\ \mathcal{D}_{61} & \mathcal{D}_{62} & \mathcal{D}_{63} & \mathcal{D}_{64} & \mathcal{D}_{65} & \mathcal{D}_{66} & \mathcal{D}_{67} & \mathcal{D}_{68} \\ 0 & 0 & 0 & 0 & W_1^{II}(1) & W_2^{II}(1) & W_3^{II}(1) & W_4^{II}(1) \\ 0 & 0 & 0 & 0 & W_1^{II'}(1) & W_2^{II'}(1) & W_3^{II'}(1) & W_4^{II'}(1) \end{vmatrix} = 0, \tag{41}$$

where the new quantities $\mathcal{D}_{ij}$ stand for

$$\mathcal{D}_{3i} := W_i^I(\eta_2), \quad i = 1,2,3,4 \quad \mathcal{D}_{3i} := -W_{i-4}^{II}(\eta_2), \quad i = 5,6,7,8.$$
$$\mathcal{D}_{4i} := W_i^{I'}(\eta_2), \quad i = 1,2,3,4 \quad \mathcal{D}_{4i} := -W_{i-4}^{II}{}'(\eta_2), \quad i = 5,6,7,8,$$
$$\mathcal{D}_{5i} := \sum_{k=1}^{4} G_{3k} W_i^{I(k-1)}(\eta_2), \quad i = 1,2,3,4, \quad \mathcal{D}_{5i} := -\sum_{k=1}^{4} H_{3k} W_{i-4}^{II\ (k-1)}(\eta_2), \quad i = 5,6,7,8,$$
$$\mathcal{D}_{6i} := \sum_{k=1}^{4} G_{4k} W_i^{I(k-1)}(\eta_2), \quad i = 1,2,3,4, \quad \mathcal{D}_{6i} := -\sum_{k=1}^{4} H_{4k} W_{i-4}^{II\ (k-1)}(\eta_2), \quad i = 5,6,7,8.$$

and the notation $(\bullet)^{(k-1)}$ denotes the $(k-1)$th-order derivative of $(\bullet)$ with respect to ρ.

The main idea is to take advantage of the presence of the two large parameters (μ and n) and simplify the above equation asymptotically. To this end, we need to use the WKB approximation in $\mu \gg 1$ and $n \gg 1$. In the former case, the differential equations (28) in $\Omega_{(j)}$ ($j \in \{I, II\}$) are amenable to asymptotic integration by adopting the ansatz

$$W^{(j)}(\rho) := \left\{ a_0^{(j)}(\rho) + \frac{1}{\mu} a_1^{(j)}(\rho) + \dots \right\} \exp\left\{ \mu \int_{\bullet}^{\rho} H^{(j)}(\zeta)\, \mathrm{d}\zeta \right\}, \quad \rho \in \Lambda_{(j)}, \tag{42}$$

where the intervals $\Lambda_{(j)}$ were defined in Section 2.2, and the lower integration limit is taken to be η_1 for Λ_I and η_2 for Λ_{II}. If (42) is substituted into the bifurcation equation (28), and then like powers of μ are collected, at leading order we get the characteristic equation for $H^{(j)}$

$$X^2 \left[X^2 - \mathring{\sigma}_{rr}^{(j)}(\rho) \right] = 0, \quad \rho \in \Lambda_{(j)}. \tag{43}$$

The distinct solutions of Equation (43) yield two linearly independent functions that can be used as approximations for $W_i^{(j)}$ ($i = 1,2$),

$$W_i^{(j)}(\rho) \simeq P_i^{(j)}(\rho) E_i^{(j)}(\rho), \quad i \in \{1,2\} \quad \text{(no sum over } i\text{)}, \tag{44}$$

in which

$$P_1^{(j)}(\rho) \equiv P_2^{(j)}(\rho) \equiv P^{(j)}(\rho) := \rho^{-1/2} \left[\mathring{\sigma}_{rr}^{(j)}(\rho) \right]^{-3/4},$$

$$E_{1,2}^{(j)}(\rho) := \exp\left\{ \pm \mu \int_{\eta_{(j)}}^{\rho} \sqrt{\mathring{\sigma}_{rr}^{(j)}(\zeta)}\, \mathrm{d}\zeta \right\}, \quad \rho \in \Lambda_{(j)}.$$

Using the assumption $1 \ll n \ll \mu$, after lengthy manipulations we conclude that

$$\frac{\mathrm{d}^i W^I_{1,2}}{\mathrm{d}\rho^i}(\eta_1) \sim \mathcal{O}(\mu^i), \quad \frac{\mathrm{d}^i W^I_{1,2}}{\mathrm{d}\rho^i}(\eta_2) \sim \mathcal{O}(\mu^i \mathcal{E}^I_{\pm}), \quad i = 0, 1, 2, 3, \tag{45a}$$

$$\frac{\mathrm{d}^i W^{II}_{1,2}}{\mathrm{d}\rho^i}(\eta_2) \sim \mathcal{O}(\mu^i), \quad \frac{\mathrm{d}^i W^{II}_{1,2}}{\mathrm{d}\rho^i}(1) \sim \mathcal{O}(\mu^i \mathcal{E}^{II}_{\pm}), \quad i = 0, 1, 2, 3, \tag{45b}$$

where

$$\mathcal{E}^{(j)}_{\pm} := \exp\left\{\pm\mu \int_{\Lambda_{(j)}} \sqrt{\mathring{\sigma}^{(j)}_{rr}(\zeta)}\, \mathrm{d}\zeta\right\}.$$

As in the related works of the first author and his associates [2, 3], it turns out that the remaining functions $W^{(j)}_3$ and $W^{(j)}_4$ in (39) can be approximated by the solutions of the reduced equations (38); to distinguish between the two sets of functions we shall keep the same notations, but will use the 'overbar' to denote the approximations.

Equations (38) can be recast in a more convenient form with the help of a standard Liouville–Green transformation

$$R^{(j)}(\rho) := \rho\, \mathring{\sigma}^{(j)}_{rr}(\rho), \quad Y^{(j)}(\rho) := \sqrt{R^{(j)}(\rho)}\, \overline{W}^{(j)}(\rho),$$

so that our original equations become

$$Y^{(j)\prime\prime}(\rho) - n^2 Q^{(j)}(\rho) Y^{(j)}(\rho) = 0, \quad (j \in \{I, II\}), \tag{46}$$

where the dash indicates differentiation with respect to ρ,

$$Q^{(j)}(\rho) := Q^{(j)}_1(\rho) + \frac{1}{n^2} Q^{(j)}_2(\rho),$$

and

$$Q^{(j)}_1 := \frac{1}{\rho R^{(j)}}\left[\frac{\delta^2}{\rho^2} + R^{(j)\prime}\right], \quad Q^{(j)}_2 := \frac{1}{4}\left\{\left[\frac{R^{(j)\prime}}{R^{(j)}}\right]^2 + 2\frac{\mathrm{d}}{\mathrm{d}\rho}\left[\frac{R^{(j)\prime}}{R^{(j)}}\right]\right\}, \quad \delta := n/\mu \ll 1.$$

The general solutions of (38) are a linear combination of the functions $\overline{W}^{(j)}_3$ and $\overline{W}^{(j)}_4$ (whose asymptotic behaviour will be discussed below),

$$\overline{W}^{(j)}(\rho) = d_3 \overline{W}^{(j)}_3(\rho) + d_4 \overline{W}^{(j)}_4(\rho), \quad (j \in \{I, II\}),$$

where $d_3, d_4 \in \mathbb{R}$ are real arbitrary constants. For the asymptotic simplification of the determinant equation (41) we are going to need the leading-order behaviour of $W^{(j)}_i$ $(i = 3, 4)$ at the boundary points $\rho_B \in \{\eta_1, \eta_2, 1\}$; at this juncture it is important to recognize that $\overline{W}^{(j)}_i$ can serve as approximations for $W^{(j)}_i$ $(i = 3, 4$ and $j \in \{I, II\})$, and this will be used tacitly henceforth. We shall use WKB arguments in (46) when $n \gg 1$.

If $Q^{(j)}(\rho_B) < 0$, then the WKB method gives

$$\overline{W}^{(j)}_3(\rho) \simeq \left[R^{(j)2}(\rho)\, |Q^{(j)}(\rho)|\right]^{-1/4} \sin(n\chi^{(j)}(\rho)),$$

$$\overline{W}^{(j)}_4(\rho) \simeq \left[R^{(j)2}(\rho)\, |Q^{(j)}(\rho)|\right]^{-1/4} \cos(n\chi^{(j)}(\rho)),$$

which are both $\mathcal{O}(1)$ quantities with respect to $n \gg 1$; here, $\chi^{(j)}(\rho) := \int_\bullet^\rho \sqrt{|Q^{(j)}(\zeta)|}\, \mathrm{d}\zeta$ and the lower integration limit is appropriately chosen. On the other hand, if now $Q(\rho_B) > 0$, then the same WKB approximations yield

$$\overline{W}^{(j)}_3(\rho) \simeq \left[R^{(j)2}(\rho) |Q^{(j)}(\rho)|\right]^{-1/4} \exp(n\chi^{(j)}(\rho)), \tag{48a}$$

$$\overline{W}^{(j)}_4(\rho) \simeq \left[R^{(j)2}(\rho) |Q^{(j)}(\rho)|\right]^{-1/4} \exp(-n\chi^{(j)}(\rho)). \tag{48b}$$

In relation to this last approximation, let us introduce some further notation,

$$\mathcal{F}_{\pm}^{(j)} := \begin{cases} \mathcal{O}(1), & \text{if } Q(\rho_B) < 0, \\ \exp\left(\pm n\chi^{(j)}(\rho_B)\right), & \text{if } Q(\rho_B) > 0. \end{cases}$$

It is clear that irrespective of whether $Q(\rho_B) < 0$ or $Q(\rho_B) > 0$ we always have $\mathcal{E}_{+}^{(j)} \ll \mathcal{F}_{+}^{(j)}$ and $\mathcal{E}_{-}^{(j)} \gg \mathcal{F}_{-}^{(j)}$, provided that also $1 \ll n \ll \mu$. Further algebraic manipulations of (48) produce the following simple estimates

$$\frac{d^i \overline{W}_3^{(j)}}{d\rho^i}(\rho) \sim \mathcal{O}(n^i \mathcal{F}_{+}), \quad \frac{d^i \overline{W}_4^{(j)}}{d\rho^i}(\rho) \sim \mathcal{O}(n^i \mathcal{F}_{-}), \quad i = 0, 1, 2, 3. \tag{49}$$

We are at last in a position to expand the 8×8 determinant in (41) by using the Laplace expansion theorem. This can be done in a number of different ways, but here we choose to carry out this procedure by using the first and the last two rows. Thus,

$$\mathcal{D}(\lambda; \mu, \nu_1, \nu_2, \eta_1, \eta_2, n) =$$

$$\sum_{\substack{1 \le p_1 < p_2 < p_3 < p_4 \le 8 \\ 1 \le q_1 < q_2 < q_3 < q_4 \le 8}} (-1)^{18+p_1+p_2+p_3+p_4} D(1,2,7,8|p_1,p_2,p_3,p_4) \cdot D(3,4,5,6|q_1,q_2,q_3,q_4), \tag{50}$$

where $p_i \neq q_j$ for any $i,j \in \{1,2,3,4\}$, and $D(i_1,i_2,i_3,i_4\,|\,j_1,j_2,j_3,j_4)$ represents the 4×4 minor formed with the elements situated at the intersections between the rows $i_1,\ldots,i_4$ and the columns $j_1,\ldots,j_4$. If we keep only the exponentially large terms in $\mathcal{E}_{+}^{I,II}$ and neglect all the terms containing $\mathcal{E}_{-}^{I,II}$, there should be one 5 and no 1, 2 among $p_1,\ldots,p_4$, and one 1 and no 2, 5 among $q_1,\ldots,q_4$. Eventually, only four leading-order terms are left

$$\mathcal{D}(\lambda; \mu, \nu_1, \nu_2, \eta_1, \eta_2, n) = -\phi_1 + \phi_2 + \phi_3 - \phi_4 + \ldots = 0, \tag{51}$$

where

$$\phi_1 := D(1,2,7,8|2,3,5,7) \cdot D(3,4,5,6|1,4,6,8), \quad \phi_2 := D(1,2,7,8|2,4,5,7) \cdot D(3,4,5,6|1,3,6,8),$$
$$\phi_3 := D(1,2,7,8|2,3,5,8) \cdot D(3,4,5,6|1,4,6,7), \quad \phi_4 := D(1,2,7,8|2,4,5,8) \cdot D(3,4,5,6|1,3,6,7),$$

and the dots stand for higher-order terms that we suspect will play only a secondary role.

The asymptotic estimates of the leading-order terms of ϕ_i $(i = 1,\ldots,4)$ are very tedious, so here we report briefly only the calculations corresponding to ϕ_1 as the other terms are handled in a similar way (a more detailed version of these derivations can be found in the PhD Thesis of the second author):

$$\phi_1 = \begin{vmatrix} W_2^I(\eta_1) & W_3^I(\eta_1) & 0 & 0 \\ W_2^{I\prime}(\eta_1) & W_3^{I\prime}(\eta_1) & 0 & 0 \\ 0 & 0 & W_1^{II}(1) & W_3^{II}(1) \\ 0 & 0 & W_1^{II\prime}(1) & W_3^{II\prime}(1) \end{vmatrix} \cdot \begin{vmatrix} \mathcal{D}_{31} & \mathcal{D}_{34} & \mathcal{D}_{36} & \mathcal{D}_{38} \\ \mathcal{D}_{41} & \mathcal{D}_{44} & \mathcal{D}_{46} & \mathcal{D}_{48} \\ \mathcal{D}_{51} & \mathcal{D}_{54} & \mathcal{D}_{56} & \mathcal{D}_{58} \\ \mathcal{D}_{61} & \mathcal{D}_{64} & \mathcal{D}_{66} & \mathcal{D}_{68} \end{vmatrix} = \Gamma_1 \Gamma_2 \Gamma_3, \tag{52}$$

where

$$\Gamma_1 := \begin{vmatrix} W_2^I(\eta_1) & W_3^I(\eta_1) \\ W_2^{I\prime}(\eta_1) & W_3^{I\prime}(\eta_1) \end{vmatrix} = \begin{vmatrix} \mathcal{O}(1) & \mathcal{O}(\mathcal{F}_{+}^I) \\ \mathcal{O}(\mu) & \mathcal{O}(n\mathcal{F}_{+}^I) \end{vmatrix} \simeq -W_2^{I\prime}(\eta_1) \cdot \overline{W}_3^I(\eta_1) + \cdots,$$

$$\Gamma_2 := \begin{vmatrix} W_1^{II}(1) & W_3^{II}(1) \\ W_1^{II\prime}(1) & W_3^{II\prime}(1) \end{vmatrix} = \begin{vmatrix} \mathcal{O}(\mathcal{E}_{+}^{II}) & \mathcal{O}(\mathcal{F}_{+}^I) \\ \mathcal{O}(\mu\mathcal{E}_{+}^{II}) & \mathcal{O}(n\mathcal{F}_{+}^I) \end{vmatrix} \simeq -W_1^{II\prime}(1) \cdot \overline{W}_3^{II}(1) + \cdots,$$

according to the information provided in (45) and (49); Γ_3 denotes the second determinant in (52) and is expanded as outlined below.

Noting that in the terms $\mathcal{D}_{ij}$ that enter in this determinant some of the $W_i^{I,II}$ and their derivatives are multiplied by n, with the assumption $1 \ll n \ll \mu$, we discover that

$$\mathcal{D}_{51} \simeq \beta_1 W_1^{I\prime\prime}(\eta_2) \sim \mathcal{O}(\mu^2 \mathcal{E}_+^I), \qquad \mathcal{D}_{54} \simeq \beta_1 \left[-\frac{n^2 \nu_1}{\eta_2^2} W_4^I(\eta_2) + W_4^{I\prime\prime}(\eta_2) \right] \sim \mathcal{O}(n^2 \mathcal{F}_-^I),$$

$$\mathcal{D}_{56} \simeq -\beta_2 W_2^{II\prime\prime}(\eta_2) \sim \mathcal{O}(\mu^2 \mathcal{E}_-^{II}), \quad \mathcal{D}_{58} \simeq -\beta_2 \left[-\frac{n^2 \nu_2}{\eta_2^2} W_4^{II}(\eta_2) + W_4^{II\prime\prime}(\eta_2) \right] \sim \mathcal{O}(n^2 \mathcal{F}_-^{II}),$$

$$\mathcal{D}_{61} \simeq \beta_1 W_1^{I\prime\prime\prime}(\eta_2) \sim \mathcal{O}(\mu^3 \mathcal{E}_+^I), \qquad \mathcal{D}_{64} \simeq \beta_1 \left[-\frac{1 + n^2(2 - \nu_1)}{\eta_2^2} W_4^{I\prime}(\eta_2) + W_4^{I\prime\prime\prime}(\eta_2) \right] \sim \mathcal{O}(n^3 \mathcal{F}_-^I),$$

$$\mathcal{D}_{66} \simeq -\beta_2 W_2^{II\prime\prime\prime}(\eta_2) \sim \mathcal{O}(\mu^3 \mathcal{E}_-^{II}), \quad \mathcal{D}_{68} \simeq -\beta_2 \left[\frac{1 + n^2(2 - \nu_2)}{\eta_2^2} W_4^{II\prime}(\eta_2) + W_4^{II\prime\prime\prime}(\eta_2) \right] \sim \mathcal{O}(n^3 \mathcal{F}_-^{II}),$$

and, hence,

$$\Gamma_3 := \mu^6 \mathcal{E}_+^I \mathcal{F}_-^I \mathcal{E}_-^{II} \mathcal{F}_-^{II} \begin{vmatrix} \mathcal{O}(1) & \mathcal{O}(1) & \mathcal{O}(1) & \mathcal{O}(1) \\ \mathcal{O}(1) & \mathcal{O}(\delta) & \mathcal{O}(1) & \mathcal{O}(\delta) \\ \mathcal{O}(1) & \mathcal{O}(\delta^2) & \mathcal{O}(1) & \mathcal{O}(\delta^2) \\ \mathcal{O}(1) & \mathcal{O}(\delta^3) & \mathcal{O}(1) & \mathcal{O}(\delta^3) \end{vmatrix};$$

recall that the constants β_j $(j = 1, 2)$ were defined at the end of Section 2.2. If we now apply the Laplace expansion for the 4×4 determinant Γ_3, the leading-order term will be $D(3,4|1,3) \cdot D(1,2|2,4)$, irrespective of whether $Q^I(\eta_2)$ and $Q^{II}(\eta_2)$ are greater or smaller than zero. Hence,

$$\Gamma_3 := -\begin{vmatrix} \mathcal{D}_{51} & \mathcal{D}_{56} \\ \mathcal{D}_{61} & \mathcal{D}_{66} \end{vmatrix} \cdot \begin{vmatrix} \mathcal{D}_{34} & \mathcal{D}_{38} \\ \mathcal{D}_{44} & \mathcal{D}_{48} \end{vmatrix} \sim -\beta_1 \beta_2 \begin{vmatrix} W_1^{I\prime\prime}(\eta_2) & W_2^{II\prime\prime}(\eta_2) \\ W_1^{I\prime\prime\prime}(\eta_2) & W_2^{II\prime\prime\prime}(\eta_2) \end{vmatrix} \cdot \begin{vmatrix} \overline{W}_4^1(\eta_2) & -\overline{W}_4^{II}(\eta_2) \\ \overline{W}_4^{I\prime}(\eta_2) & -\overline{W}_4^{II\prime}(\eta_2) \end{vmatrix}.$$

It can be shown that putting together the asymptotic estimates for ϕ_i $(i = 1, \ldots, 4)$, Equation (51) becomes

$$-\begin{vmatrix} \overline{W}_3^I(\eta_1) & 0 \\ 0 & \overline{W}_3^{II}(1) \end{vmatrix} \cdot \begin{vmatrix} \overline{W}_4^I(\eta_2) & -\overline{W}_4^{II}(\eta_2) \\ \overline{W}_4^{I\prime}(\eta_2) & -\overline{W}_4^{II\prime}(\eta_2) \end{vmatrix} + \begin{vmatrix} \overline{W}_3^I(\eta_1) & 0 \\ 0 & \overline{W}_4^{II}(1) \end{vmatrix} \cdot \begin{vmatrix} \overline{W}_4^I(\eta_2) & -\overline{W}_3^{II}(\eta_2) \\ \overline{W}_4^{I\prime}(\eta_2) & -\overline{W}_3^{II\prime}(\eta_2) \end{vmatrix}$$

$$+\begin{vmatrix} \overline{W}_4^I(\eta_1) & 0 \\ 0 & \overline{W}_3^{II}(1) \end{vmatrix} \cdot \begin{vmatrix} \overline{W}_3^I(\eta_2) & -\overline{W}_4^{II}(\eta_2) \\ \overline{W}_3^{I\prime}(\eta_2) & -\overline{W}_4^{II\prime}(\eta_2) \end{vmatrix} + \begin{vmatrix} \overline{W}_4^I(\eta_1) & 0 \\ 0 & \overline{W}_4^{II}(1) \end{vmatrix} \cdot \begin{vmatrix} \overline{W}_3^I(\eta_2) & -\overline{W}_3^{II}(\eta_2) \\ \overline{W}_3^{I\prime}(\eta_2) & -\overline{W}_3^{II\prime}(\eta_2) \end{vmatrix}$$

$$+ \ldots = 0.$$

A close inspection of the above equation reveals that, to leading order, the original determinant condition (41) is equivalent to

$$\begin{vmatrix} \overline{W}_3^I(\eta_1) & \overline{W}_4^I(\eta_1) & 0 & 0 \\ \overline{W}_3^I(\eta_2) & \overline{W}_4^I(\eta_2) & -\overline{W}_3^{II}(\eta_2) & -\overline{W}_4^{II}(\eta_2) \\ \overline{W}_3^{I\prime}(\eta_2) & \overline{W}_4^{I\prime}(\eta_2) & -\overline{W}_3^{II\prime}(\eta_2) & -\overline{W}_4^{II\prime}(\eta_2) \\ 0 & 0 & \overline{W}_3^{II}(1) & \overline{W}_4^{II}(1) \end{vmatrix} = 0,$$

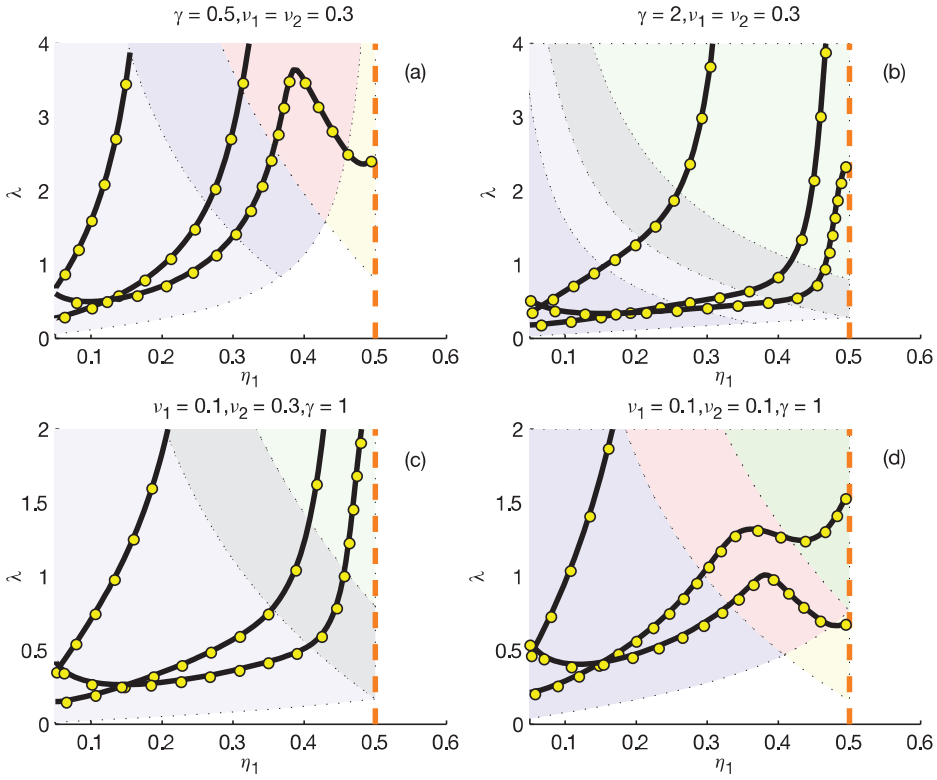

Figure 13. Comparisons between the numerical solutions of the reduced problem, (38) complemented by (54) (*yellow circles*), and the original problem, (28) and (34) (*black continuous lines*). In all four windows: $\mu = 400.0$, $\eta_2 = 0.5$ and the three solid black curves shown correspond to $n = 5, 20, 50$. More specifically, (a) and (d) show the kink-type response curves, while (b) and (c) illustrate the monotonic-type behaviour. The values of the parameters γ, ν_1, and ν_2 are specified in the titles of the subplots, and the coloured background follows the conventions outlined in Table 1.

which is precisely the determinant equation for (38) corresponding to the constraints

$$\overline{W}^{I}(\eta_1) = 0, \qquad \overline{W}^{II}(1) = 0, \tag{54a}$$

$$\overline{W}^{I}(\eta_2) = \overline{W}^{II}(\eta_2), \quad \frac{\mathrm{d}\overline{W}^{I}}{\mathrm{d}\rho}(\eta_2) = \frac{\mathrm{d}\overline{W}^{II}}{\mathrm{d}\rho}(\eta_2). \tag{54b}$$

Incidentally, this is also the right number of constraints required to solve (38).

We solved the reduced equations (38) in Ω_I and Ω_{II}, subject to the simplified boundary constraints (54a) and the interfacial matching conditions (54b). The interface is situated at $\eta_2 = 0.5$ and the large parameter is taken to be $\mu = 400.0$ in all of our examples; from an asymptotic point of view the latter value is only moderate. As our extensive numerical experiments (not included here for the sake of brevity) have indicated, larger values of μ tend to lead to even more accurate results. The captions of the plots included below give full information about the values of the other parameters used in our comparisons.

In all plots in Figure 13, as η_1 increases from the initial value 0.1 to $\eta_2 = 0.5$ (the location of the interface), the four sets of curves shown there are almost indistinguishable for a range of values of γ, ν_1 and ν_2. As a side note, we see that these response curves are traversing differently coloured regions (corresponding to the basic state classification in Table 1), but the accuracy between numerics and asymptotics is hardly affected by this aspect. In the interest of brevity we have included only the case $\eta_2 = 0.5$, although comparable results are obtained for other interface locations. In conclusion, it is clear that our reduced model performs admirably well for moderate values of μ and mode numbers as low as $n = 5$ (which is well outside the range of our original assumption, $n \gg 1$).

6. Conclusions

The problem of tensile wrinkling for a radially stretched thin annular plate discussed by Coman and Haughton [2] has been extended to a system consisting of two (mechanically different) concentric annular plates perfectly bonded along a circular interface. The initial motivation behind this study came from trying to understand whether the localized wrinkling observed in the previous experimental studies by Geminard et al. [1, 2] can be counteracted (or at least limited) by adopting plates with piecewise-constant mechanical properties. This simple question turned out to necessitate a fairly laborious analysis of bi-annular plates, and revealed a series of unexpected results.

By using a coordinate-free variational approach we have established the correct form of the Weierstrass–Erdmann "corner" conditions for the so-called bi-annular plate; previous researchers seem to have got this wrong (see [4, 5]). These allowed us to match the solutions of the linearized Föppl–von Kármán equations that were applicable in each of the two sub-annular regions. Wrinkling instabilities were then studied with the help of a normal-mode approach by using both direct numerical simulations and an asymptotic reduction technique first proposed by Coman and Haughton [2], and that was later adapted to successfully cope with a wide variety of problems [3, 22, 23]. In particular, we have discovered that in the limit $\mu \gg 1$ the complicated fourth-order three-point boundary eigenproblem describing wrinkling can be understood in terms of two second-order ordinary differential equations whose solutions had to be matched along the interface. As in the earlier case of a simple stretched annulus, we have made extensive use of the WKB method to simplify a complicated 8×8 determinant equation. In a recent related work [10], the first author has showed how uniform asymptotic approximations of these equations can actually lead to relatively simple analytical approximations for the critical loads.

Here, for the sake of simplicity the interface between the two sub-annular regions of the plate was assumed to be perfect. It would be of interest to understand how the coupling between the two regions affects the wrinkling load. One possible extension of the present study would be to consider that the constituent parts are connected through a ring, in a similar way to the problem discussed by Frosting and Simitses [5]. A more rigorous way to account for imperfect interfaces would be to consider that the original annular domain Ω consists not only of Ω_I and Ω_{II} as in this paper, but also of a third (very) narrow annular region Ω_m "squeezed" between them. This is akin to the problem of adhesively bonded joints (e.g. see Movchan and Movchan [24]), but it is more complicated because of the need to identify the critical eigenvalues and due to the higher order of the differential equations involved. These problems are currently under investigation and will be reported elsewhere.

Conflict of interest

None declared.

Funding

This work was supported by the Engineering and Physical Sciences Research Council (grant number EP/F035136) while the senior author (CDC) was based in Glasgow. The second author acknowledges with gratitude the financial support of a Studentship associated with the above grant, and he would also like to thank the University of Glasgow for some additional financial support.

Notes

1. Without loss of generality we disregard in-plane variations at this stage because the equations describing the in-plane deformations can be solved independently of the buckling problem for the out-of-plane displacement, w.

References

[1] Géminard, JC, Bernal, R, and Melo, F. Wrinkle formations in axis-symmetrically stretched membranes. *Eur Phys J E* 2004; 15: 117–126.

[2] Coman, CD, and Haughton, DM. Localised wrinkling instabilities in radially stretched annular thin films. *Acta Mech* 2006; 185: 179–200.

[3] Coman, CD, and Bassom, AP. On the wrinkling of a pre-stressed annular thin film in tension. *J Mech Phys Solids* 2007; 55: 1601–1617.

[4] Frostig, Y, and Simites, GJ. Buckling of multi-annular plates. *Comput Struct* 1986; 24(3): 443–454.

[5] Frostig, Y, and Simites, GJ. Buckling of ring-stiffened multi-annular plates. *Comput Struct* 1988; 29(3): 519–526.
[6] Simitses, GJ. Effect of boundary conditions and rigidities on the buckling of annular plates. *Thin-Walled Struct* 1987; 5(4): 229–246.
[7] Stavsky, Y, and Greenberg, JB. Axisymmetric vibrations of concentric dissimilar isotropic composite plates. *Comput B: Engng* 1999; 30(6): 553–567.
[8] Stavsky, Y, and Greenberg, JB. Axisymmetric vibrations of concentric dissimilar orthotropic composite annular plates. *J Sound Vibr* 2002; 254(5): 849–865.
[9] Elishakoff, I, Li, Y, and Starnes, JH, Jr. *Non-classical Problems in the Theory of Elastic Stability*. Cambridge: Cambridge University Press, 2001.
[10] Coman, CD. Some applications of the WKB method to the wrinkling of bi-annular plates in tension. *Acta Mechanica* 2013; 224(2): 399–423.
[11] Roccabianca, S, Bigoni, D, and Gei, M. Long wavelength bifurcations and multiple neutral axes of elastic layered structures subject to finite bending. *J Mech Mat Struct* 2010; 6(1-4): 511–527.
[12] Roccabianca, S, Gei, M, and Bigoni, D. Plane strain bifurcations of elastic layered structures subject to finite bending: theory versus experiments. *IMA J Appl Math* 2010; 75(4): 525–548.
[13] Steele, CR, and Skogh, J. Slope discontinuities in pressure vessels. *ASME J Appl Mech* 1970; 37: 587–595.
[14] Gelfand, IM, and Fomin, SV. *Calculus of Variations.* Mineola, NY: Dover Publications, 2000.
[15] Auzinger, W, Kneisl, G, Koch, O, and Weinmüller, E. Sbvp 1.0 - *a* MATLAB *solver for singular boundary value problems*. Technical report, Institute for Applied Mathematics and Numerical Analysis, 2002. Available at: http://www.math.tuwien.ac.at/∼ewa/.
[16] Auzinger, W, Kneisl, G, Koch, O, and Weinmüller, E. A collocation code for singular boundary value problems in ordinary differential equations. *Numer Algorithms* 2003; 33: 27–39.
[17] Koch, D, Auzinger, W, Karner, E, and Weinmüller, E. Collocation methods for the solution of eigenvalue problems for singular ordinary differential equations. *Opuscula Math* 2006; 26(2): 229–241.
[18] Ascher, U, and Russell, RD. Reformulation of boundary-value problems into "standard" form. *SIAM Rev* 1981; 23(2): 238–254.
[19] Lindsay, KA. The application of compound matrices to convection problems in multi-layered continua. *Math Models Meth Appl Sci* 1992; 2(2): 121–141.
[20] Coman, CD, and Haughton, DM. On some approximate methods for tensile instabilities of thin annular plates. *J Engng Math* 2006; 56(1): 79–99.
[21] Coman, CD, and Bassom, AP. Singular behaviour in a generalised BVP for annular plates in tension. *Quart J Mech Appl Math* 2007; 60(3): 319–336.
[22] Coman, CD. Elastic instabilities caused by stress concentration. *Int J Engng Sci* 2008; 46(9): 877–890.
[23] Coman, CD. Remarks on elastic buckling for sectorial plates. *Int J Engng Sci* 2009; 47(10): 1002–1013.
[24] Movchan, AB, and Movchan, NV. *Mathematical Modelling of Solids with Non-regular Boundaries.* Boca Raton, FL: CRC Press, 1995.